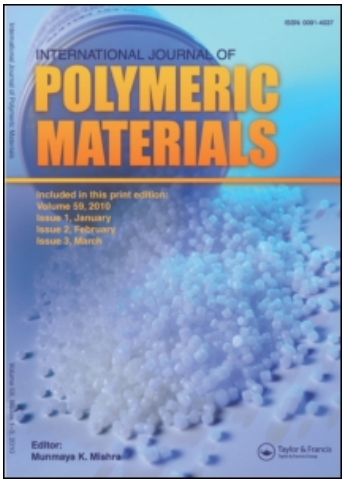

International Journal of Polymeric Materials
Publication details, including instructions for authors and subscription information:
http://www.informaworld.com/smpp/title~content=t713647664

Synchrotron Radiation for Probing the Electric Field Alignment of LC Macromolecules and Polymers

Timothy J. Bunning[a]; Wade Adams[a]; Christopher K. Ober[b]; Hilmar Korner[b]
[a] Materials Directorate, OH, USA [b] Department of Materials Science and Engineering, Cornell University, Ithaca, NY, USA

To cite this Article Bunning, Timothy J. , Adams, Wade , Ober, Christopher K. and Korner, Hilmar(2000) 'Synchrotron Radiation for Probing the Electric Field Alignment of LC Macromolecules and Polymers', International Journal of Polymeric Materials, 45: 3, 451 — 501
To link to this Article: DOI: 10.1080/00914030008035051
URL: http://dx.doi.org/10.1080/00914030008035051

Intern. J. Polymeric Mater., 2000, Vol. 45, pp. 451–501
Reprints available directly from the publisher
Photocopying permitted by license only

Synchrotron Radiation for Probing the Electric Field Alignment of LC Macromolecules and Polymers

TIMOTHY J. BUNNING[a,*], WADE ADAMS[a], CHRISTOPHER K. OBER[b] and HILMAR KORNER[b]

[a] *Materials Directorate, Wright-Patterson AFB, OH 45433-7702, USA;*
[b] *Department of Materials Science and Engineering, Cornell University, Ithaca, NY 14853, USA*

(Received 18 December 1998)

The use of synchrotron radiation to probe non-equilibrium electric-field mediated structures is analyzed for a variety of liquid crystalline (LC) systems. Examples are provided for monomer LCs (MLCs) and for a variety of polymer LCs (PLCs) including comb and network PLCs. Monitoring both response and relaxation times of induced ordering, the resultant orientation parameters, correlation lengths, dynamic behavior of alignment and reorientation processes are reported as a function of time, temperature and frequency for a number of systems.

Keywords: Synchrotron radiation; non-equilibrium electric-field mediated structures; monomer liquid crystals; MLCs; polymer liquid crystals; PLCs; comb PLCs; network PLCs; relaxation times of induced ordering; orientation parameters; correlation lengths; LC alignment; reorientation processes

1. INTRODUCTION

The purpose of this paper is to describe the use of synchrotron radiation to probe the nonequilibrium, electric field mediated structures of the liquid crystalline phase in a variety of liquid crystalline systems. Conventional X-ray sources, both fixed and rotating anode, do not have sufficient intensity to permit monitoring of microstructural and

*e-mail: Timothy.Bunning@afrl.af.mil

molecular changes in real time. Given that the constituent atoms of the material have small scattering cross-sections for X-rays, it is only by using the high flux of radiation available from a synchrotron source that these dynamic and transient structures can be observed. The high flux of X-ray radiation from a synchrotron source allows for time resolved X-ray diffraction (TRXRD) experiments to be performed on a system where alignment occurs over millisecond and greater time scales. Eventually, with new detector designs, even faster molecular responses will be able to be probed.

The majority of this paper describes examples of this technique applied to a variety of material systems. These include monomer liquid crystals (MLCs), hybrid liquid crystals, and polymer liquid crystals (PLCs), both comb PLCs and network PLCs. First, a general overview of the experimental procedures used to obtain the research data will be given. Examples from each class of these materials are shown, especially those from our work since we know of no other work yet reported. Examples of monitoring both response and relaxation times of induced ordering, the resultant orientation parameters and correlation lengths, as well as dynamic behavior of alignment and reorientation processes are given as a function of time, temperature, and frequency for a number of systems. In addition, examples of monitoring very complex phase behavior, surface effects on alignment, dynamic crystallization from an induced aligned mesophase, and the evolution of oriented mesophases during a chemical reaction are shown. All of these examples will not be explored for a given material system; instead selections from the various material systems are used to show a particular type of data and interpretation that can be obtained. We feel that the information that can be obtained using synchrotron radiation is important to a wide variety of applications, since many uses of liquid crystalline materials in industry are predicated on the ability to align them. As applied electric fields are finding more and more use, it is helpful to better understand the microstructural changes LC systems undergo while in such fields. The processing of LC systems can be better designed when such relationships are fed back into the design loop of material synthesis and characterization. Experimental details will be given only when needed; otherwise appropriate references will be highlighted. Finally, a perspective on the significance of these studies will be given in the final

section of the article. Developments critical to the future of this characterization technique will be highlighted and other dynamic information that may be possibly obtained will be discussed.

2. BACKGROUND

The use of synchrotron radiation in polymer science has grown considerably over the last five to ten years. Although static scattering techniques allow considerable information to be obtained about polymer microstructure, details about the time evolution of these microstructures cannot be easily obtained. The high X-ray flux of synchrotron sources allows dynamic processes to be examined in real-time, providing vital information necessary in the development and processing of new materials. Using synchrotron radiation, both small angle (SAXS) and wide-angle X-ray scattering (WAXS) information can be obtained simultaneously, often within seconds. This technique has been widely used to examine changes in scattering during crystallization, melting, and deformation of a variety of polymer types. Because the time resolution of the technique is on the order of time changes used in the processing of such systems, useful insight into key variables during processing can be obtained.

In the last two decades, several simultaneous synchrotron techniques such as SAXS/WAXD/small-angle laser scattering (SALS) [1] SAXS/DSC, [2, 3] and WAXD/DSC [4] and SAXS/FT-IR [5] have been developed. These techniques have demonstrated the unique capabilities of synchrotron X-ray diffraction in the study of phase transitions in polymers. Fundamental examination of the crystallization and melting kinetics of unaligned samples on a variety of material systems have been reported in the literature [6–17]. Effects of physical deformation and annealing on the microstructure and morphology of polymer materials is key to their development into useful films and fibers for commercial use. A considerable amount of work has been performed on examining structural changes during fiber spinning of various polymers [7, 18–22]. Examination of the degree of spatial alignment across a sample correlated with spinning variables gives insight into optimization of properties and processing conditions [23]. Dependence of both draw rates and temperatures on the development

of crystallinity and orientation can be monitored. This information is particularly useful in industrial production where identification of temperatures over which optimal properties are developed is of interest. Other geometries are possible as evidenced by the examination of films (tapes) of various materials during stretching and annealing experiments. Monitoring the phase separation processes of block co-polymers in real time leads to an increased understanding of the thermodynamic incompatibility driving microstructural development [24–30]. Simultaneous SAXS/WAXS/DSC has also been applied to study the phase transitions in semi-crystalline and amorphous polyurethanes wherein a similar thermodynamic incompatibility leads to a separation of hard and soft segments and thus microphase separation [31]. Changes in structure during reactive processing can also be obtained and this evolution of structure may be related to changes in molecular weight [5, 32]. A correlation between reaction kinetics and structure development as well as other morphological changes can be determined.

The use of synchrotron radiation in the examination of both MLC and PLC material systems has also been an area of significant study. Time resolved diffraction techniques were carried out to examine the complex phase behavior of a number of lyotropic LC systems. A high flux synchrotron source has been used in the investigations of the dynamics and mechanisms of biological liquid crystal phase transitions in bulk systems. Fine reviews of such work have been published [33, 34]. More recent work has continued with the use of the high flux to monitor laser-induced rapid heating and its effect on the kinetics and structural mechanisms of thermotropic phase transitions in a phospholipid/water system [35]. Attempts have been made to examine the correlation of structural changes using simultaneous calorimetry and synchrotron radiation [36], to obtain time-resolved optical and diffraction information on membrane lipids [37], to follow the time evolution of magnetically induced growth of biological macromolecules [38], and to structurally characterize a variety of lipid and membrane systems [39–41].

A number of papers examining real-time structural characterization of thermotropic LC systems have also been published. Nonequilibrium shear-flow effects on the phase transitions of MLCs have been explored [42–47]. The effect of processing conditions on PLC

systems has been investigated for a variety of systems including liquid crystalline polyesters [23, 48–52], rigid-rod polymers [53], copolyester [54] and polybenzoxazole [55, 56] fiber spinning, and general characterization of thin liquid crystalline films [57–64] under both equilibrium and dynamic conditions. All these experiments serve to demonstrate that synchrotron scattering techniques may be used as effective structural probes of dynamic processes inherent to or induced in LC systems.

3. LCs AND ELECTRIC FIELDS

The orientation of MLCs and PLCs with an applied electric or magnetic field is a well known phenomenon [65, 66]. Coupling of the electro-and magneto-responsive properties of the MLC mesogens with the robust physical properties of polymer systems may be advantageous for many applications. PLCs as a class of materials have been very successful as high performance fibers and injection moulded components [67]. Comb PLCs are presently being investigated as they combine physical properties common to polymers (glass-forming, film forming, and good optical and dielectric properties) with properties common to liquid crystals (electroactive, magnetoactive, and variable optical properties) [68]. The ability to macroscopically align and then vitrify order into the glassy state provides a method of introducing spatial contrast into thin films which is useful for applications such as data storage, nonlinear optical devices, display devices [68–74]. Reversibility can be obtained by heating above the glass transition temperature, thereby 'erasing' the contrast. Macroscopically aligned films can be formed using electric and magnetic fields or surface treatment of substrates. A greater understanding of the development of the structure present within these materials during processing is desired.

The alignment properties of these compounds in electric fields are controlled by their dielectric anisotropy, defined as the difference between the two dielectric permittivities ε_{11} and $\varepsilon\perp$. These permittivities are dependent on chemical structure, sample purity, temperature, and frequency [65, 75]. A typical plot of these two permittivities as a function of frequency is shown in Figure 1a. As shown in this figure, a crossover frequency may exist where the sign of the anisotropy

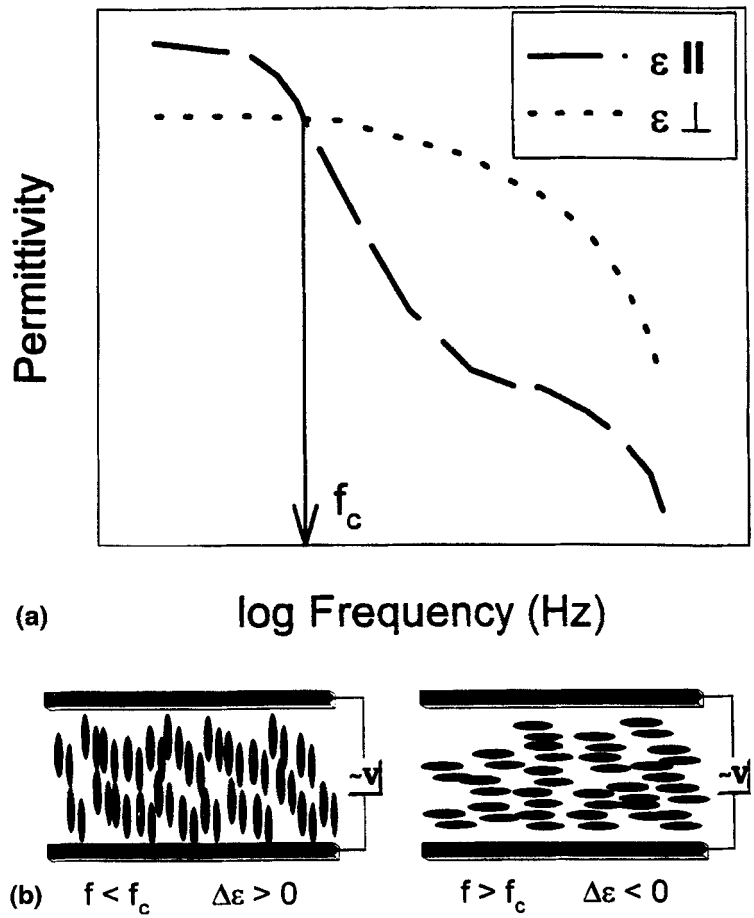

FIGURE 1 (a) Frequency dependence of the two dielectric permittivities defining a crossover frequency where the sign of the dielectric anisotropy changes and (b) the resulting alignment characteristics of a material system above and below this crossover frequency.

changes from positive to negative. This crossover frequency is the basis of the dual-frequency effect in MLCs as shown in Figure 1b. A strong electric field below the crossover frequency results in a homeotropic alignment of directors (long axis of molecules parallel to applied field directions). The strength of the applied field has to be above a

threshold-voltage which depends on the properties of the LC material. Above this frequency, planar alignment is induced. A marked temperature dependence of the crossover frequency is typically observed for PLCs as the reorientational motions of the dipolar mesogenic groups occur in an co-operative manner in a highly viscous environment, and as the glass transition temperature is approached these motions undergo a critical slowing similar to that observed for the α-relaxation in amorphous solid polymers [76]. A thorough review of the intricacies of alignment of comb PLCs in electric fields has been published [76 – 79].

Alignment of comb PLCs can be accomplished from either the mesophase or the isotropic melt although the mechanism for alignment is fundamentally different in each case [76]. The dynamics of the realignment of a LC material in an applied field have been described by a continuum theory as outlined in the literature [80, 81]. The magnitude and kinetics of steady-state orientation of the realignment of a LC molecules have been investigated using these equations [82, 83]. The reorientation of a LC material involves both flow of the mesophase and reorientation of the director axes. If flow is suppressed by crosslinking, then the alignment properties will be greatly affected. For steady state alignment when flow has ceased, a plateau level of alignment will be reached when the dielectric forces are balanced by the elastic forces of the phase. For electric-field alignment, differences in the dielectric anisotropy as a function of frequency and temperature are typically used to induce planar or homeotropic orientation of the director with respect to a substrate [75]. The strong frequency dependence of the dielectric constants of polar mesogens allows for switching between the two orientations. This can convert the molecular anisotropy of the mesogens into a macroscopic anisotropy. However, under the influence of external fields these materials are usually not in thermodynamic equilibrium. Non-equilibrium conditions can lead to dramatically different arrangements of the mesogens with potential effects on optical, mechanical, and viscoelastic properties. We focus our attention on the use of applied electric fields to develop and characterize aligned LC structures.

A number of ways of probing the director alignment have been used including polarized light optical microscopy (POM) [77, 84, 85] and dielectric spectroscopy (DRS) [78, 86]. The DRS technique depends on assumptions about the electronic structure of the mesogens and POM

yields information on the macroscopic scale. Neither method yields molecular-based structural information on the organization of the LC phase although DRS are ideally suited for MLC systems where the response times are typically fast (< 1 ms).

Static X-ray diffraction techniques are extensively and routinely used to investigate the degree of order and molecular packing of the mesogens after alignment. The distinctive X-ray scattering of aligned LC phases has served as a tool for many years in the identification and characterization of the packing of anisotropic molecules. Many texts and reviews of X-ray scattering from PLC exist [87–90]. By aligning the domains of the LC mesophase, the coherent scattering of X-rays from the material is increased and identification of the structure facilitated. Even though the response times of PLC compounds are typically 10 to 1000 times slower (milliseconds to minutes) due to the increased viscosity compared to MLCs, X-ray experiments on these systems still cannot yield time resolved information about the alignment kinetics and structural transformation due to the long exposure times needed with ordinary X-ray sources.

The use of synchrotron radiation to explore the mesophase behavior of PLCs under the influence of an applied field is relatively new. In fact, only one other group to our knowledge has performed comparable work [91]. In it, they examine the simultaneous observation of small angle X-ray patterns and time dependent birefringence changes of a monomer smectic liquid crystal cell. The gathering of simultaneous data on two fronts maximizes information from a single experiment. Similar to our beliefs, they state that the physics of LCP systems under the influence of applied fields can be much better understood *via* study of the dynamics of switching behavior. The work presented in this article highlights a variety of experiments involving electric fields and synchrotron radiation on numerous material systems.

4. EXPERIMENTAL PROCEDURES

X-ray diffraction data were obtained at various beamlines of the Cornell High Energy Synchrotron Source (CHESS). Sample cells consisted of two 0.5 mm gold-plated stainless steel electrodes separated by a controlled gap spacing of 100–200 μm (Fig. 2a) which were held

in a Mettler FP82HT hotstage. Samples were melted between the electrodes and held in place by capillary forces. A schematic of the sample relative to the incoming radiation is shown in Figure 2b.

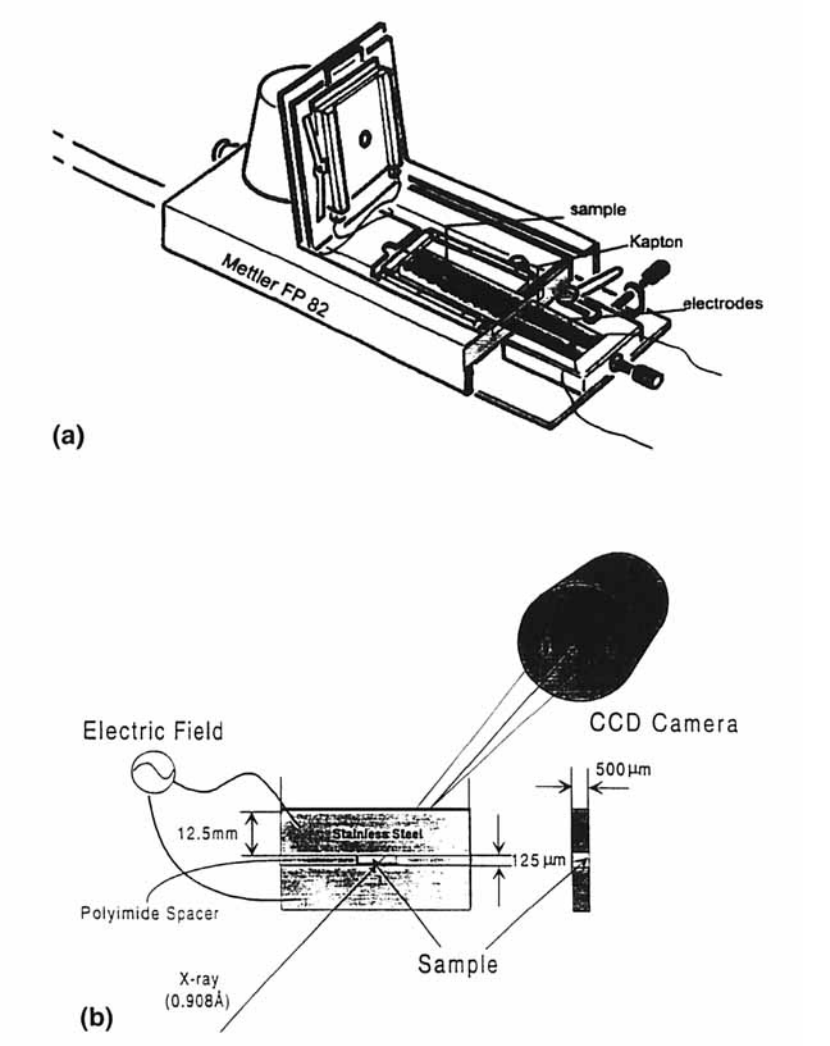

FIGURE 2 (a) Schematic of the Mettler hot-stage with the two electrodes in place, (b) orientation of the hot-stage and sample relative to the incoming radiation and (c) overall experimental setup for the electric field alignment, heating, and X-ray data collections on LC material systems.

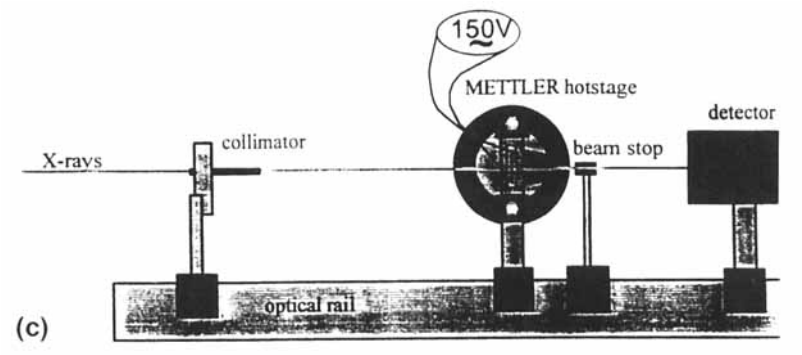

FIGURE 2 (Continued).

Voltage and frequency of the applied field were controlled by passing the output from an HP 3300A function generator through a high voltage operational amplifier (Trek, model 10/10). Voltages typically employed varied between 0 – 300 V and the frequencies of interest have up to this point been 1 – 10000 Hz. Many of the molecules examined to date are based on ester linkaged mesogens which typically have switching values within the applied range of frequencies. Nothing however fundamentally limits the voltage (except dielectric breakdown) or frequency space that may be examined. The samples in the hot-stage were placed on an optical rail as shown in Figure 2c. A translation stage, mounted to hold the samples perpendicular to the X-ray beam, moved the hotstage within the beam.

Various detectors have been used throughout the course of this work. Real-time images were obtained by collecting the diffracted radiation using an image intensifier coupled to a digital video camera. This allows frame rates of 1/30 sec to be obtained. Problems with this approach are that only a very small solid angle of diffracted radiation can be obtained (*i.e.*, one cannot collect data from small angle and wide angle regions simultaneously). Scattering patterns were collected and stored on *U*-matic format video tape for storage and subsequent analysis. The collected solid angle of radiation of the image intensifier was small (2θ: 0 – 6°) and typically only the small-angle reflection was fully recorded.

One dimensional images using an OMA II positional sensitive detector have also been obtained. This type of detector is useful for the rapid characterization of unaligned samples which show complex

phase behavior within narrow temperature ranges. This type of detector can be useful for oriented samples only if the orientation relative to the electric field is known. The profile of the aligned reflection can be probed as a function of the field variables.

The latest detector being employed for fast capturing of the scattering patterns is a charge-coupled device (CCD) camera which greatly enhances the linear resolution of the data. It does severely curtail the time resolution of the experiments in its present format however. Changes on the time scale of 20 seconds can be examined with this detector. Although individual exposures 0.1 seconds in duration can be obtained, the readout rate of the camera is on the order of 15–20 seconds.

Flat-film (Kodak DEF) or image plates were also used to selectively record diffraction patterns. Exposure times varied from 0.1 sec to 20 sec for the film depending on the flux of incident X-rays which was monitored using a N_2 ion chamber (10 cc/min, 1 cm flight path). Examples of all four types of detector data will be shown in the subsequent discussions.

Typical procedures involved cooling to the desired temperature from the isotropic phase. The voltage was applied and changes in the small-angle reflection were recorded on videotape until a steady state was achieved. The image intensifier was removed and a flat-film photograph was taken at this point of alignment. The image intensifier was replaced, the field turned off, and the relaxation was monitored on video tape (only alignment data will be discussed here). The sample was heated to the isotropic phase, to erase any thermal history effects, and cooled to the next temperature of interest. Switching experiments were done either by cooling through the transition temperature or by cooling at one frequency and then switching the frequency to facilitate domain rotation. Typically, the image intensifier was used to obtain time-resolved information although the OMA II detector has been used also. For accurate determination of microstructural parameters (orientation parameters (S_d) and correlation lengths (L_{string} or L_{DS}), CCD or flat-film data was used. L_{string} refers to the one dimensional correlation of columns while L_{DS} refers to the layer correlation (estimated using the Debye-Scherrer equation) as discussed in detail previously [92, 93]. Differentiation of the orientation parameter (S_d) *versus* the order parameter (s) is described in the next section.

An RCI Framestore image processor was used in conjunction with a commercially available image processing software package to analyze the digitized data from the image intensifier. Data sets in the form of intensity *versus* x, y pixel position were captured as frames from the videotape. CCD images were analyzed using subroutines developed with a mathematical software program. All necessary corrections were performed on the images before orientation parameters and correlation lengths were obtained. Details of these calculations can be found in previously published work [92, 93].

For all X-ray patterns presented here, the direction of the aligning field was vertical. Orientation parameters are reported as positive for a homeotropic orientation and negative for a planar orientation. Values were calculated relative to the molecular director in each case (not relative to the E-field direction). Negative values for planar orientations were used to indicate that a switch from the predominant homeotropic orientation relative to the electrodes had occurred. Within the context of our experimental geometry, the term "homeotropic" refers to the arrangement of the long axis of the mesogens parallel to the applied field and perpendicular to the electrodes, while "planar" represents the arrangement of the mesogens perpendicular to the applied field and parallel to the electrodes.

5. MATERIAL SYSTEMS EXAMINED

5.1. Monomer Liquid Crystals

Figure 3 shows the chemical structure of three MLCs discussed in this section along with their thermal transitions. Compound I is a precursor to a main-chain PLC while compounds II and III are dimer-based molecules with much different mesophase behaviors. Figure 4 shows one dimensional data taken by the OMA detector from compound I as it was heated through its complicated mesophase. Melting to a higher ordered smectic occurs at 114°C, followed by a transition to a S_A phase and then further development into a nematic phase before clearing. Some of these subtle transitions can be easily missed on the light microscope but are clearly evident using a high flux synchrotron source. Although transitions can be missed using X-ray

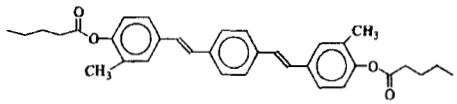

I: k 114 S_G 165 S_A 180 n 285 i

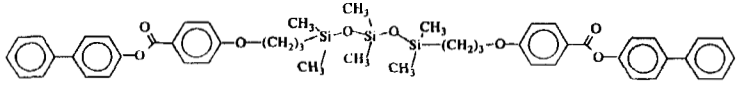

II: k_1 76 k_2 118 i
i 94 n 89 S_A 64 k_1

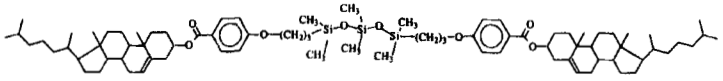

III: k 80 S_A 220 i

FIGURE 3 Chemical structures and thermal transitions of three monomer liquid crystalline systems (compounds I, II and III).

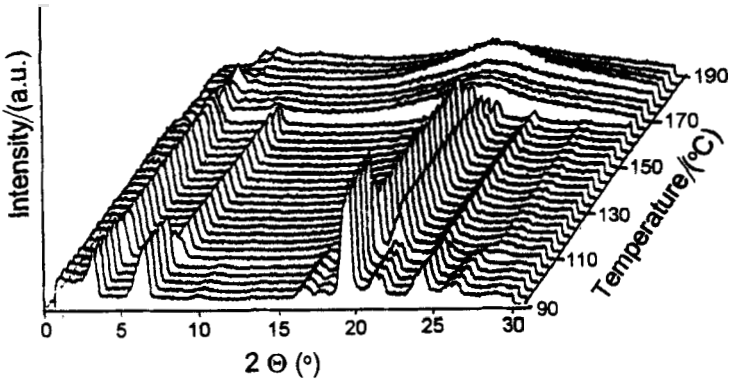

FIGURE 4 One dimensional X-ray scattering curves from compound I as it is heated at 20°C per minute from 90°C to 190°C. Scans were taken at 5 sec intervals. (adapted from [94]).

techniques as well, its combination with proper optical microscopy increases the chances of proper characterization. One can also examine the time dependence of the structural transformations of these phase transitions when the sample is either unaligned or aligned. Indeed, polymers formed from this system have been aligned and the dynamics of the orientation process have been described elsewhere [94].

When applying an electric field to this model compound, measurement of the orientation was easily achieved as shown in Figure 5. Changes from a positive to negative orientation parameter can be interpreted as two types of alignment; the first being indicative of parallel alignment of the long axis of the mesogen with the applied electric field while the second is indicative of perpendicular alignment. This difference in orientation will be addressed more thoroughly in the next section. A large dependence on the degree of alignment with frequency is also observed. For 100 Hz, a relatively large orientation parameter in the smectic phase is observed which, after heating the sample, slowly decreases as the nematic transition temperature is approached. Before this transition, a switch in the orientation from perpendicular (as evidenced by the negative orientation parameter) to parallel is observed. This behavior can be contrasted to that exhibited at 1000 Hz which shows little temperature dependence of the orientation parameter as the nematic transition temperature is approached. More importantly, it should be emphasized that this orientation and other effects were not evident optically. At such temperatures, the material appeared immobile under the microscope. As the alignment data indicates, this was clearly

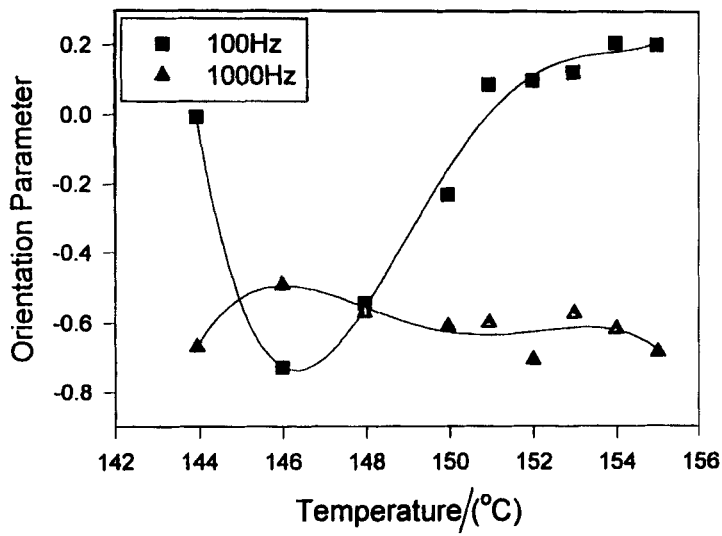

FIGURE 5 The alignment response of compound I in the smectic mesophase upon cooling at two different frequencies. (adapted from [94]).

not the case which shows the importance of being able to probe the microstructure using X-ray diffraction techniques.

Compound II consists of two biphenyl-based mesogens attached to a short siloxane core. This material exhibits a monotropic phase and was examined upon cooling from the isotropic phase. Being one of the first compounds examined by us at the synchrotron, basic information regarding response and relaxation times and frequency dependence of alignment were probed. Typical alignment data is shown in Figure 6 from the nematic phase at 10 Hz. The experimental response curves observed in this study exhibit a two-part response, an initial fast alignment process followed by a second, slower alignment process. Although we are using an AC field, we observe responses to the field similar to those associated with a DC field [82, 83] increasing alignment occurs until steady state is obtained. It is speculated that the induced dipoles within the system cannot respond at the frequency of the AC field. In twisted nematic field effect (TNFE) cells, this phenomenon is due to the accumulation of electric energy in the cell [75]. The response times to achieve steady state orientation can be calculated by fitting the data collected with the image intensifier to Eq. (1) below. S_d refers to the orientation parameter, a measure of the macroscopic

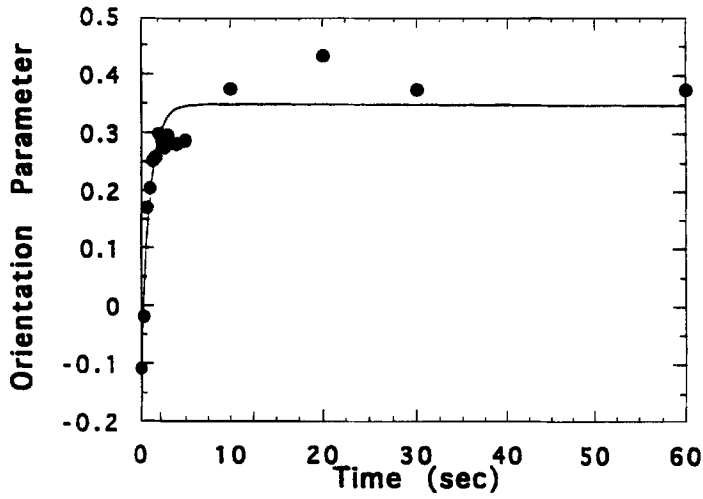

FIGURE 6 Evolution of the orientation parameter as a function of time for compound II at 91°C using a frequency of 10 Hz. The line through the data points shows a fit using Eq. (1) to obtain a value for the response time.

alignment of the system. If one assume equilibrium alignment, then S_d becomes the equivalent of s, the order parameter. However, this assumption of equivalence should not be made generically in systems where orientation is changing under a variety of conditions (not all of which are equilibrium) and so this distinction is noted.

$$S_d = m_1 + m_2\left(1 - \exp\left(-t/\tau_r\right)\right) \tag{1}$$

Equation (1) is a variant of the standard equation used to fit conventional response time data from light microscopy measurements [65] with m_1 corresponding to the $t = 0$ value, m_2 a measure of the steady state change in S_d, and τ_r corresponding to the response time of the system. The line shown in Figure 6 is fit to the data with a response time of approximately 1 sec. The initial negative S_d indicates an initial surface orientation which caused the molecules to lie parallel to the electrode surface. By turning the field off, the realignment of the aligned LC domains can be monitored in real time as well. Figure 7 shows an example for this type of data for the same sample aligned at 10,000 Hz. The orientation parameter decreases with time until a slight surface anchoring is evident. Since relaxation behavior is only

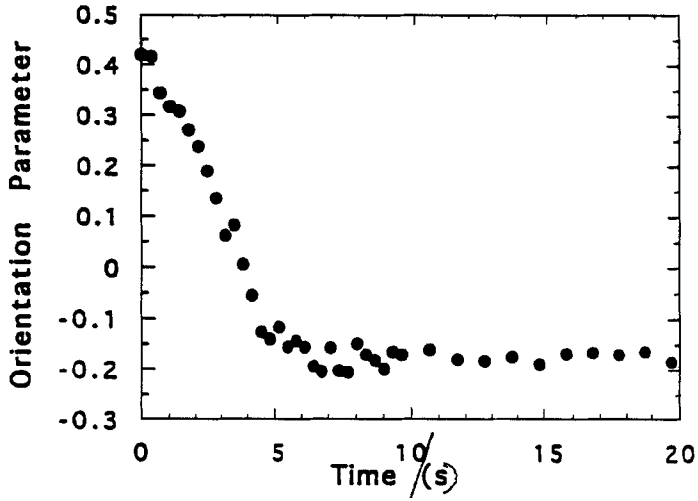

FIGURE 7 The relaxation behavior of compound II after the field is turned off at 91°C from a sample aligned at 10000 Hz.

dependent on fundamental material constants, one could extract pertinent information about specific molecular parameters. Relative correlation among molecules can also be obtained by examining in detail the shape of the Bragg reflections.

The third example examines the surface anchoring ability of compound III which consists of two cholesterol molecules attached through a short siloxane core. This compound only exhibits a smectic phase and the fact that an electric field affects the induced orientation in such a strong manner was unexpected. Interest in cholesterol containing molecules derives from the fact that they facilitate LC phase formation and the development of cholesteric phases [95, 96]. In particular, we are interested in the tendency of cholesterol containing materials to spontaneously form homeotropic films which can be used for optical applications [97, 98]. Figure 8 shows a diffraction pattern from

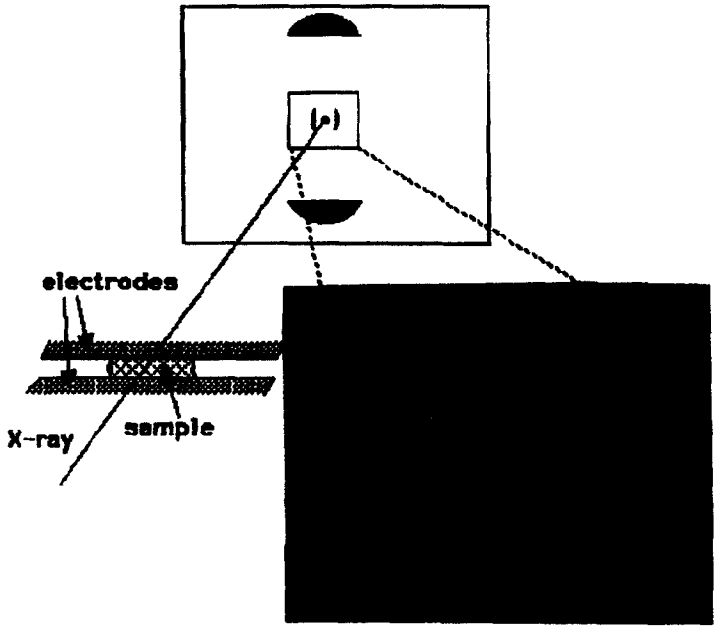

FIGURE 8 The diffraction pattern observed from compound III from the smectic phase WITHOUT an applied field relative to the sample electrodes. The strong equatorial alignment is due to surface effects. The inset shows the small angle reflection at 3.3 nm captured with an image intensifier.

a sample relative to the electrode surfaces but without an applied electric field in the smectic phase. The inset shows the small angle reflection as captured using the image intensifier is strongly aligned on the equator. This orientation indicates that very strong spontaneous alignment of the molecules parallel to the electrode surfaces takes place. The *d*-spacing of the smectic layer corresponds to 3.3 nm, roughly half the length of the molecule. The strong surface anchoring is driven by microgrooves on the inside surface of each electrode formed when the electrodes are polished.

When an applied field (1 V/μm) is maintained across the sample, strong changes in the clearing temperature are observed as well as the relative orientation of the small angle reflection. Table I shows the observed clearing temperatures as measured by the appearance of this reflection upon heating and cooling as a function of frequency. DSC indicates that the clearing temperature is 220°C without the field applied. The reflection disappears near this temperature indicating an elimination of the smectic ordering. Application of the electric field while heating to or cooling from the isotropic region depresses the observed clearing temperature. The largest effect occurred for the lowest frequencies as a 40°C suppression in the transition temperature is observed on cooling. Thus the field is acting to supercool the sample even though LC phases typically supercool by only very small amounts.

The much lower transition temperature is due to the fact that the field is trying to align the molecules parallel (orthogonal to the surface-induced direction). The competition between parallel and perpendicular orientation most likely results in a confusion of the molecules causing pseudo-isotropic behavior. Note, the field is not destroying orientation as the small angle reflection disappears entirely except for the faint halo characteristic of the isotropic phase. In this temperature

TABLE I Observed clearing temperatures (°C) for compound III on heating and cooling with applied field of varying frequency

Frequency (Hz)	*Heating*	*Cooling*
no field	220	210
100	215	180
10	200	170
1	205	175

range where the strong smectic reflections are suppressed, transient spots on both the equator and meridian appear briefly indicating a bimodal orientation of LC domains occurs. The four spots in the small angle pattern indicate domains aligned either with the field or aligned with the surface. Stable homeotropic alignment could not be obtained with this material system.

The ability to examine the structural interplay of an alignment field and surface induced effects does not otherwise exist except with synchrotron radiation due to its high flux. By understanding the prevalent surface phenomena and by characterizing this behavior on the molecular scale, one can better design systems to either couple with or resist outside external stimuli such as an electric field. The large change in the apparent transition temperatures indicates that a proper understanding of the molecular factors controlling these interactions is needed. This example shows the importance of being able to examine dynamic phenomena on the molecular scale.

5.2. Hybrid Liquid Crystals

Of particular interest are a class of materials which consist of an excluded volume core with attached mesogens [99 – 101]. The reduced melt viscosity of MLCs in the mesophase combined with the glass-forming propensity (above room temperature) of PLCs are both characteristics of hybrid low molar mass liquid crystals [102]. This combination of properties has advantages in the fabrication of uniform thin films with useful optical applications [103]. We show here some results on a series of compounds with a basic chemical structure as shown in Figure 9. These consist of simple siloxane rings with biphenyl-ester mesogens attached through various spacer group lengths.

Compound IV has been examined in detail and highlights of the results published elsewhere [92, 93, 104] are shown here. Representative diffraction patterns at various frequencies and temperatures are shown in Figure 10. These patterns consist of wide-angle crescents at scattering angles characteristic of the average lateral packing distance of the side chain mesogens (0.45 – 0.55 nm). Orthogonal to these wide-angle reflections are periodic reflections with a primary spacing of approximately 2.3 nm. The complexity of the diffraction patterns is

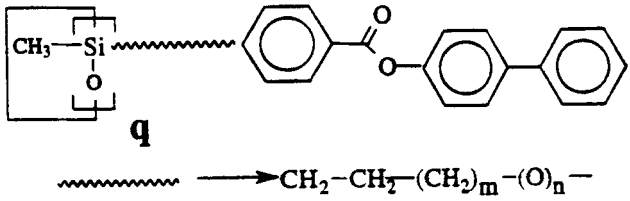

IV: q=5, m=1, n=1; i 175 n 112 k
V: q=4, m=1, n=1; i 200 n 180 k
VI: q=5, m=3, n=1; i 172 n 140 S_A 120 k

FIGURE 9 Molecular structures and thermal transition temperatures for three hybrid liquid crystal molecules (compound IV, V and VI) examined. These materials consist of a cyclic siloxane core onto which are attached a varying number of mesogens through various length spacer units.

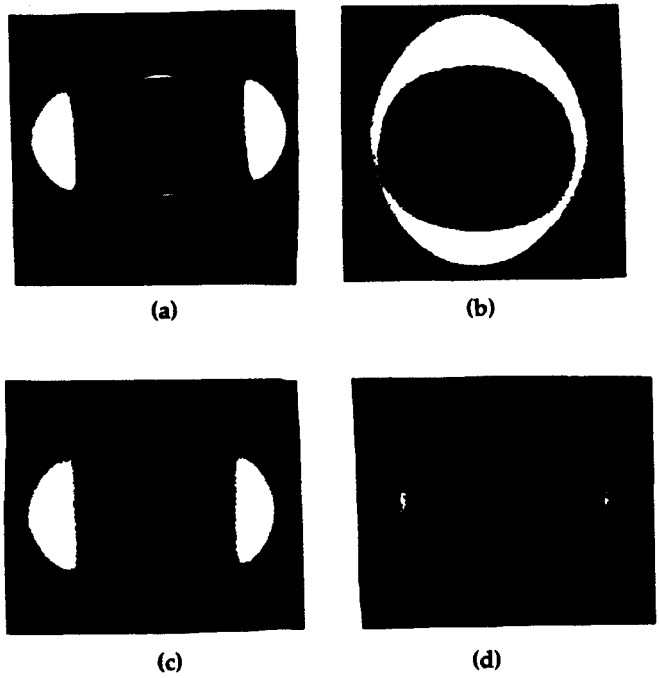

FIGURE 10 Diffraction patterns from compound IV with the electric field (a) at 120°C and 10 Hz, (b) 120°C and 10 kHz, (c) 170°C and 10 Hz, and (d) 170°C and 10 kHz. The large crescents are centered at a spacing of 0.4–0.5 nm. Orthogonal to these crescents, a series of periodic diffuse reflections exist with the inner most reflection having a spacing of 2.3 nm. (adapted from [92]).

unusual for a nematic LC and suggests molecular association among molecules is present. At 10 Hz and 120°C, the molecular director is parallel to the E-field direction and corresponds to homeotropic alignment of the mesogenic groups relative to the electrodes. At 10000 Hz and 120°C, a switch in orientation is observed as the director aligned perpendicular to the E-field direction. In this planar orientation the mesogenic groups are parallel to the electrodes as indicated by the WAXS reflections. This switch in orientation, similar to that briefly discussed for compound I, is due to the frequency dependence of the dielectric anisotropy, $\Delta\varepsilon$. As the temperature approached the clearing temperatures, only parallel alignment of the mesogens was observed. The spacings did not change significantly upon reorientation. The unaligned sample shows a typical nematic diffraction pattern which indicates the complex molecular structure exhibited here is the result of the *e*-field induced alignment process.

One can use the high flux to examine both the alignment characteristics and the reorientation behavior in real time. This processing information is important in the development of these systems for thin film optical elements. Proper processing can be used to better align the systems and remove defects. A series of experiments have been performed to examine the frequency and temperature dependence of the alignment characteristics. Director orientation parameters as a function of either temperature or frequency are shown in Figures 11a and 11b respectively. The frequency dependence of S_d at a given temperature, shown in Figure 11b, is weak through the mesophase region except at temperatures where switching occurred. For the electric field used in this study, orientation parameters ranged from 0.3 to 0.55 with the highest values being observed in the middle of the mesopase range (140°C and 150°C). For a given frequency, the orientation parameter first increased and then decreased as temperature was increased as shown in Figure 11a. This was true even at the high frequencies where switching had occurred. The lower orientation parameters at lower temperatures can be attributed to an increase in the viscosity of the mesophase such that the side chain mesogens are not as free to respond to the applied field. The loss of order at higher temperatures is consistent with Maier-Saupe theory in that the thermal fluctuations within the system overwhelm the ordering fields as T_i is approached.

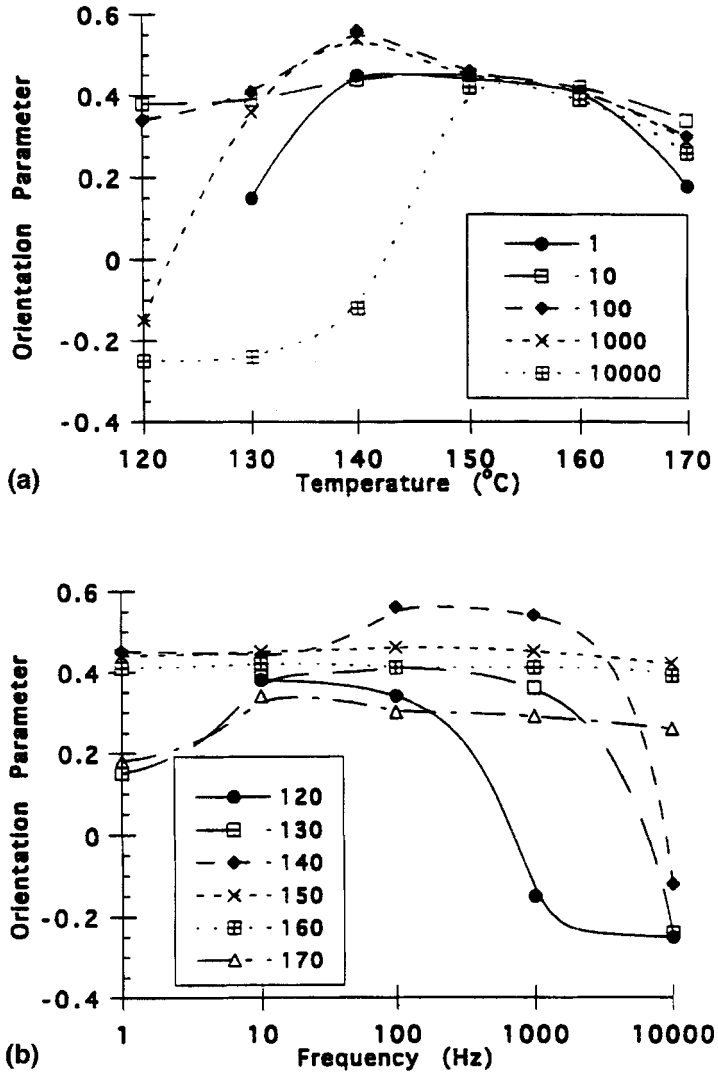

FIGURE 11 Director orientation parameters S_d as a function of temperature (a) and frequency (b) for compound IV throughout the nematic phase. (adapted from [93]).

The experimental response curves observed in this study also exhibit a two-part response (an initially fast increase in the alignment followed by a slower second increase) as discussed in subsection 5.1. Shown in Figure 12 are the fitted response times as a function of frequency and

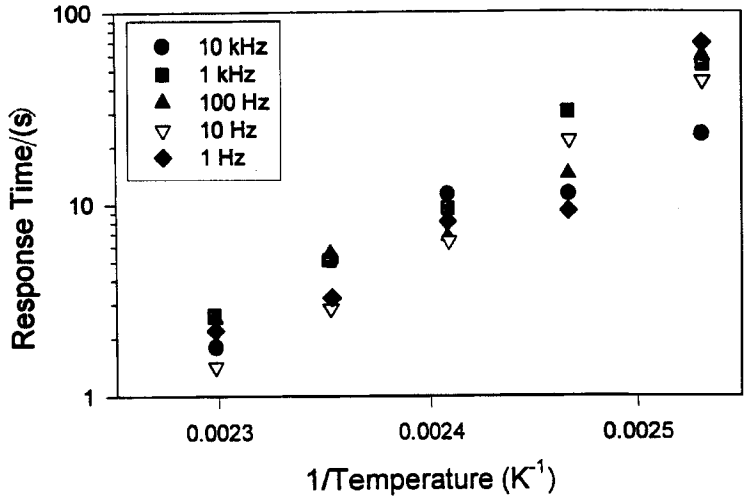

FIGURE 12 Response times as obtained from a fitting of the data from compound IV using Eq. (1) as a function of temperature and frequency. (adapted from [93]).

temperature. The rate at which the sample is able to align increases markedly with temperature as shown. The response times spanned several orders of magnitude from tenths of a second to several tens of seconds depending on temperature. These switching dynamics from planar to homeotropic alignment in conventional LMW cells is described by Eq. (2) [86],

$$\frac{1}{\tau_r} = \frac{k_{11}}{\eta_1}\left(\frac{\pi}{d}\right)^2\left(\left(\frac{U}{U_0}\right)^2 - 1\right) \tag{2}$$

where U_0 is the threshold voltage, U is the voltage, d is the sample thickness, k_{11} is the splay constant, η_1 is the viscosity, and τ_r is the response time. For this work at constant voltage, the response time should be proportional to the ratio of the splay constant to the viscosity. Since the viscosity is expected to decrease exponentially with increasing temperature and the elastic constant typically decreases linearly with temperature, one would expect the response times to decrease exponentially with increasing temperature. This is the case as shown in Figure 12. Similar to the S_d values, there is little dependence of the response times on frequency for a given temperature.

Figure 13 shows a series of images from compound IV cooled to the low end of the nematic phase at 10 Hz and then switched to 10000 Hz. During the isothermal transition from homeotropic to planar alignment, the small-angle diffraction pattern observed with the image intensifier became much more complicated. The initial two equatorial wide-angle reflections at 0° and 180° split into 4 reflections which

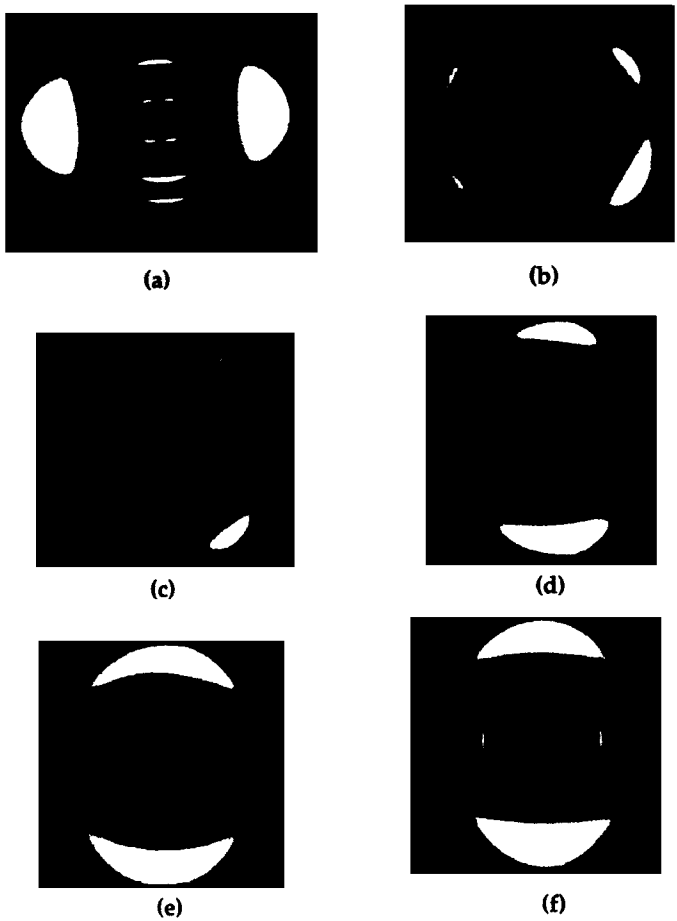

FIGURE 13 WAXS photographs as a function of time during reorientation of compound IV from homeotropic alignment to planar alignment. Note the splitting of the reflections at the intermediate times. (a) $t = 0$, (b) $t = 60$ sec, (c) $t = 105$ sec, (d) $t = 180$, (e) $t = 210$ sec, and (f) $t = 300$ sec. (adapted from [93]).

migrated azimuthally until they merge into 2 reflections at 90° and 270°, orthogonal to the original two reflections as shown in Figure 14. The orientation parameter decreases as indicated by the weakening and broadening of these reflections. A well defined split of each of the two wide-angle reflections occurs at about 1 minute and recombination occurs around 3.5 minutes. This is dramatically shown in the flat film data in Figure 13. Once recombined, the orientation parameter (director orthogonal to the original direction) increases as indicated by the increase in the intensity of the two wide-angle reflections at initial times. The splitting into four reflections is caused by the director in domains rotating in directions opposite each other.

Examination of the scattering patterns allows molecular scale structural information to be obtained in addition to information about the response parameters. Details on methodology and definitions of layer and column correlation lengths have previously been explained

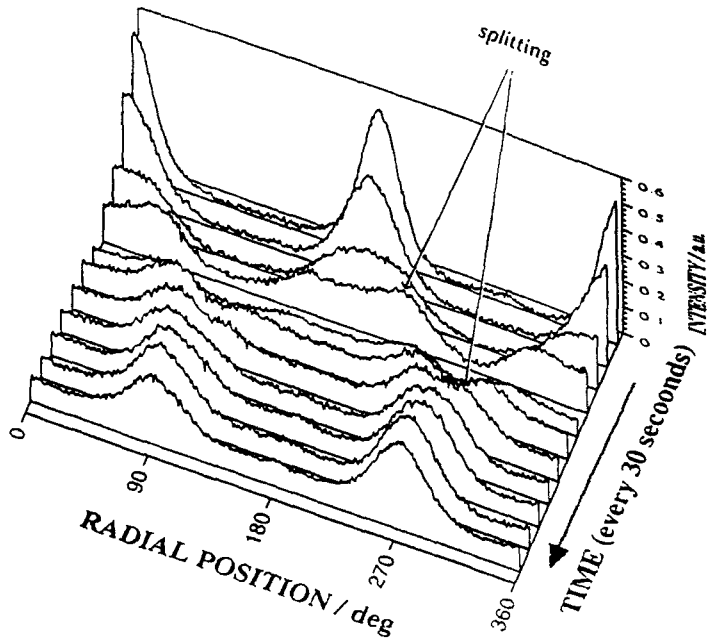

FIGURE 14 Reorientation of the wide-angle reflections as a function of time when frequency is switched from 10 to 10000 Hz for compound IV at 120°C. (adapted from [93]).

in great detail [89, 92]. Microstructural information cannot be obtained from macroscopic measurements as no correlation between order parameter (macroscopic) and correlation (microscopic) lengths are present. This lack of correlation is shown in Figure 15. The column lengths for a sample aligned at 10 Hz steadily increases with decreasing temperature from a value of $L = 6$ nm near the isotropic state to a value of $L = 12.4$ nm at 120°C. This monotonic increase can be contrasted with relatively small changes of the orientation parameter through the same temperature range as shown in the figure. Thus, examination and interpretation of structure based on orientation parameter can be flawed. Upon cooling at 10000 Hz, a marked reduction of the column-like association occurs when reorientation takes place below 145°C. This reduction can be clearly seen when the column lengths obtained from steady state alignment are plotted as a function of temperature as shown in Figure 16. The ability to do real-time scattering with high X-ray flux is advantageous as both molecular and domain structure information can be obtained as a function of time. Bulk order parameter measurements as obtained with POM do not yield information about the molecular organization of ordered phases.

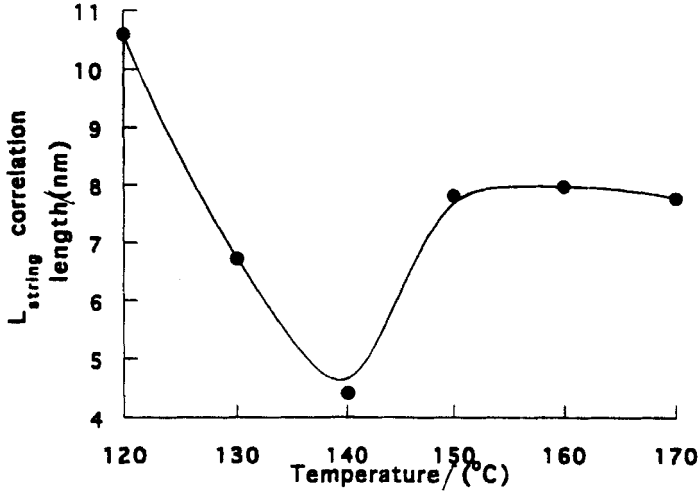

FIGURE 15 Comparison of the change in the column length for compound IV with temperature to the relatively high fixed degree of orientation across the mesophase range.

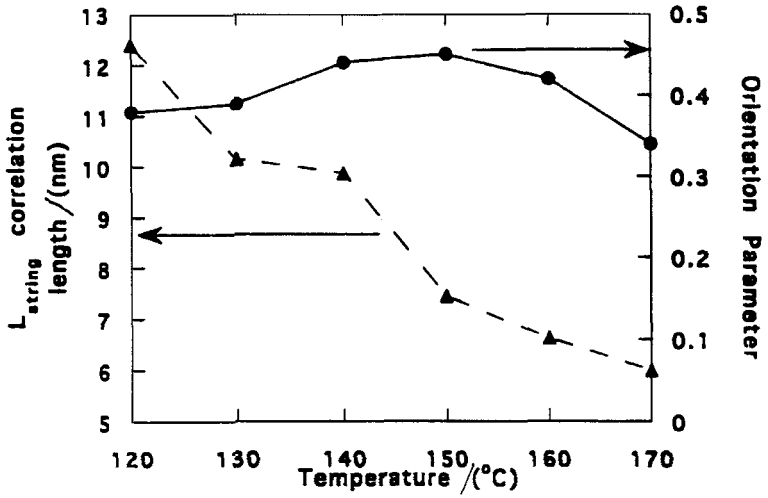

FIGURE 16 Column correlation lengths every 10 degrees upon cooling from the isotropic phase at 10000 Hz. The large decrease in the middle of the mesophase range indicates a reorientation from homeotropic to planar alignment. (adapted from [92]).

Similarly, conventional diffraction techniques would not allow for a real-time investigation of structural rearrangements and structure development.

One can also look at the effect of very small structural changes in the molecules to examine the effect of molecular architecture. All data shown in this section so far has been from compound IV. Compounds V and VI, one possessing a smaller ring size and one possessing a longer spacer group, were also aligned in the electric field in their nematic phases at both 10 and 10000 Hz [105]. Compound V only shows alignment parallel to the electric field at all frequencies. Weak periodic reflections are present indicative of a molecular association similar to compound IV. Compound VI shows a more complex behavior. At 10 Hz, weak periodic reflections are not present and alignment was perpendicular to the applied electric field throughout the nematic and smectic regions. This was unexpected given the similarities of the biphenyl-ester mesogens. At 10000 Hz, strong alignment is observed and periodic diffuse reflections persist through the nematic phase. In addition, a switch in this orientation similar to compound I was present as shown in Figure 17. Table II shows a comparison of the orientation

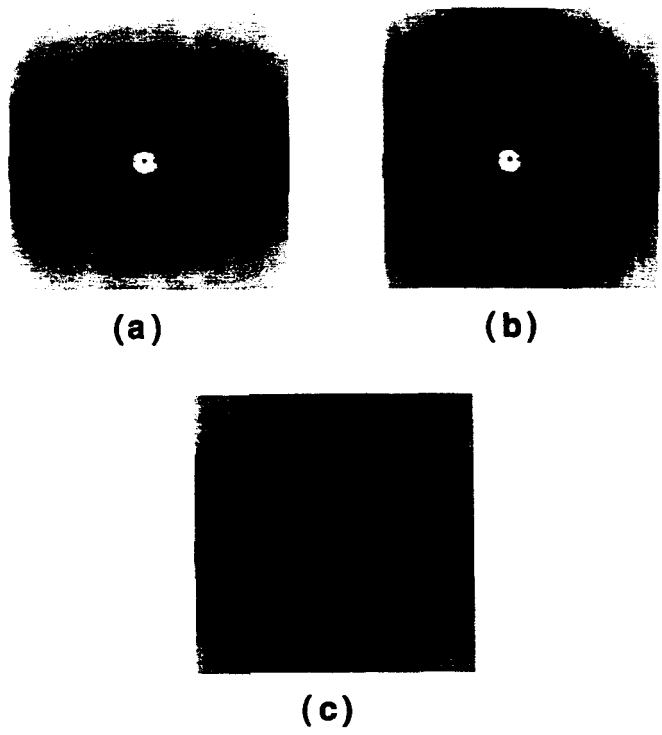

FIGURE 17 X-ray CCD images from compound VI showing strong association in the nematic phase (a); a change in the director orientation while in the nematic phase upon subsequent cooling by 5°C (b); and strong alignment when cooled into the smectic phase (c). The samples have been aligned using a frequency of 10000 Hz.

TABLE II Orientation parameters and column (L_{string}) and layer (L_{DS}) correlation lengths (nm) for compounds IV, V, and VI

	10 *Hz*			10000 *Hz*		
Compound	S_d	L_{string}	L_{DS}	S_d	L_{string}	L_{DS}
IV	0.55	14.0	4.3	0.25	8.9	2.8
V	0.62	7.6	2.4	0.65	7.8	2.4
VI	0.40	not present	4.9	0.71	30.0	9.3

parameters, correlation lengths, and the appearance of periodic reflections. Although only subtle differences in the molecular architectures are present, large differences in their packing parameters exist. No apparent correlation among the three values is observed.

These examples show the importance of using synchrotron radiation to obtain structural information necessary in the design of new molecules. In this section, although very similar structures are shown and all can be aligned and orientation parameters obtained, large differences in the packing are demonstrated. Slight differences in molecular architecture have been shown to greatly affect not only the alignment characteristics but also the degree of molecular association which can be present at different levels. By examining molecular structures using synchrotron radiation, better design of molecules with desired architectures can be conceived. The real-time measurement characteristic allows one to observe how different processing conditions change the local environment. Also obtained is information about the evolution of the structure under various constraints. We have seen that by adjusting the frequency of an applied electric field, one may address frequency dependent dielectric anisotropies that exist within a liquid crystalline material and thereby produce mesomorphic melts with very different levels of order. Such observations can now be made using X-ray scattering to directly observe the structures involved during molecular rearrangements. While this frequency dependence has been the basis of much of the technology surrounding MLCs, it is hoped that it will prove useful in the development of new technologies using PLCs as well.

5.3. Comb PLCs

Solutions to technical problems and an understanding of the way in which the complex microstructures of PLCs evolve depend on an understanding of dynamics in the mesophase and at phase transitions. These studies of liquid crystalline materials are therefore of great theoretical and experimental relevance [106]. However, whereas much work has been done on the thermodynamics of such phase transitions, very little is known of their kinetic features. From a scientific point of view, the dynamics of thermotropic polymers provide largely unexplored and technologically relevant territory for polymer physics. The use of synchrotron X-ray radiation makes time-resolved diffraction measurements possible, thus allowing for the analysis of either structural variations as the sample undergoes a phase transition or short-lived transient states, in contrast to conventional static diffraction

techniques. A system of poly(malonates) discussed here is known to have a rather flexible backbone leading to crystalline or semi-crystalline polymers upon cooling to room-temperature. The structure of the side-group poly(malonates) studied here is shown in Figure 18. From a homologous series with spacers from 3 to 12 methylene groups, only three members will be presented which show unusual crystallization behavior when cooled down in an electric field of about $1-2\,V/\mu m$. Previous studies on these polymers showed very good alignment in a magnetic field or by drawing fibers [107]. X-ray investigations were done with conventional X-ray sources and exposure times of 2 days were common so that a thorough study of the crystallization process was impossible. X-ray patterns of the smectic and crystalline phases suggested a common picture of crystallization from a LC to a solid phase where smectic layer spacings decrease due to a reduction of thermal fluctuations and where growth of the third dimension within the packing can be seen by an increase of the number of reflections.

Compound VII was melted into the isotropic phase between the electrodes and cooled down into the smectic A phase at 80°C. This polymer also exhibits a narrow nematic phase on cooling in the temperature range from 105 to 103°C. The X-ray pattern from the smectic mesophase is shown in Figure 19a at 80°C. There are several dipoles present in the structure of this class of materials. The strongest dipole is the cyano group attached as the end function of the last phenyl ring. Based on many experiments performed by us over the years using field strengths of approximately $1\,V/\mu m$, it was doubtful whether these linear polymers with polar end groups attached to the side-groups

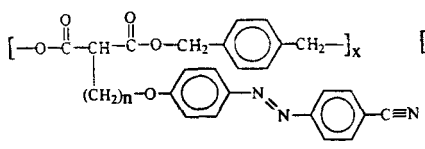

VII (n=12): k 60 S_A 103 n 105 i
VIII (n=7): g 43 S_A 107 n 128 i

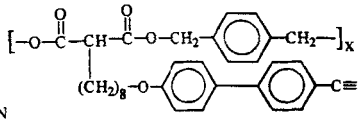

IX (n=8): k 37 S_A 85 n 97 i

FIGURE 18 Structure and transition temperatures for three poly(malonates) investigated. Compound VII has $n = 12$, compound VIII has $n = 7$, and compound IX has $n = 8$.

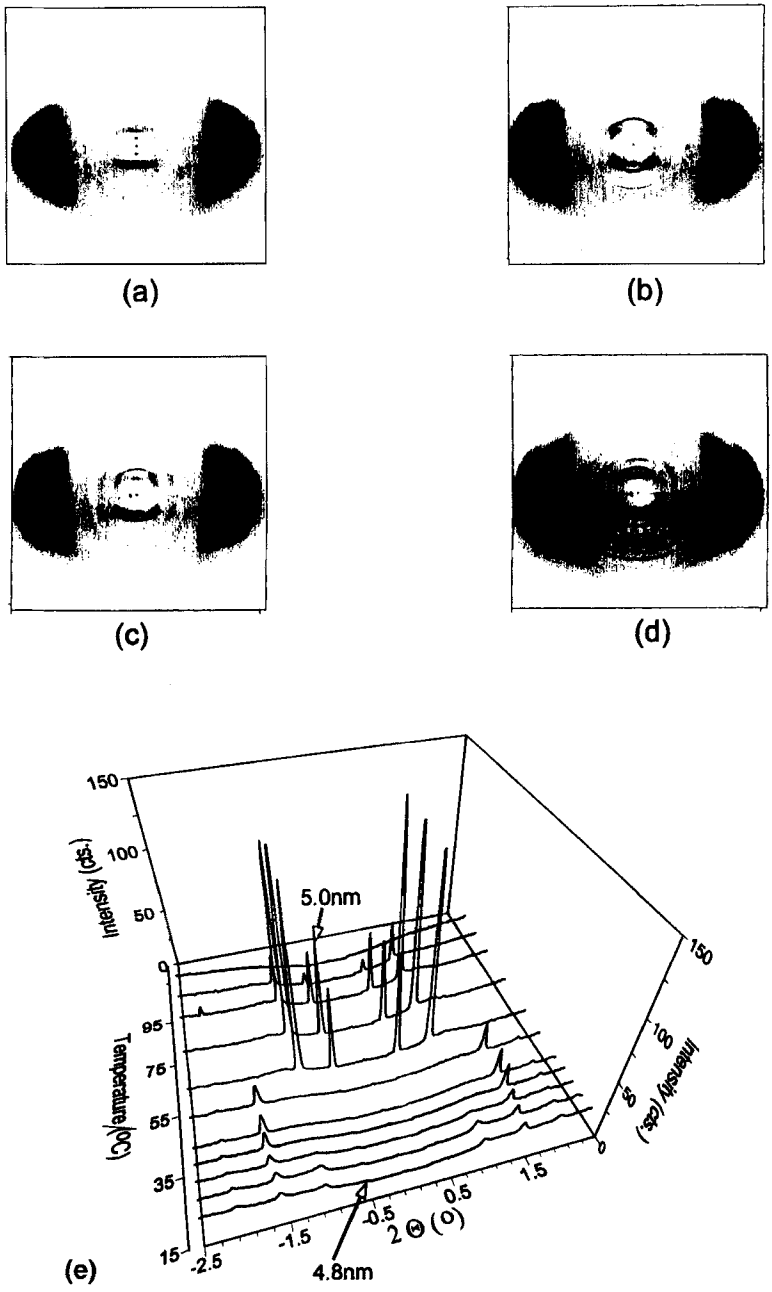

FIGURE 19 X-ray patterns of compound VII at (a) 80°C, (b) 60°C, (c) 50°C, and (d) 35°C. Meridional line scans of as a function of temperature throughout the mesophase are shown in (e).

would show any appreciable alignment. As observed however, strong alignment was induced parallel to the field direction. A change in frequency from 0.01 to 10,000 Hz did not change the X-ray pattern and the alignment of the director was in all cases parallel to the electric field. In the applied frequency window the strong dipole along the molecular axis dominates the orientation of the molecules and a coupling of the AC field with the perpendicular dipole was not observed. A closer look at the X-ray pattern of the nematic phase not shown here shows two orders of diffuse scattering maxima along the meridian. These diffuse reflections are due to intramolecular association prevalent in many PLC systems [89]. The *d*-spacing of the maxima do not correspond to the length of a side-group which is expected for such a polar molecule. Overlap of the mesogens driven by the strong dipole-dipole interactions in the nematic phase leads to *d*-spacings approximately 1.5 to 1.7 times higher than calculated from molecular models.

Further cooling into the smectic A phase leads to the X-ray pattern shown in Figure 19a. Although the formation of smectic layers leads to two strong and sharp Bragg reflections with *d*-spacings of 5.0 nm and 2.5 nm for the first and second order, the diffuse scattering maxima coexist. Upon crystallization at 60°C a very unusual behavior is obtained reflected in the disappearance of the sharp, strong layer reflections as shown in Figures 19 b, c, d. This disappearance occurs simultaneously with the emergence of a set of higher order reflections of a semi-crystalline phase. This can be better seen in Figure 19e where line scans through the meridian are plotted *versus* intensity and temperature. Another feature of the three dimensional packing is the appearance of row-lines along the meridian, parallel to the electric field. The first row-line in 19c has a *d*-spacing of 2.3 nm. This row-line could not be observed by static X-ray investigations. Figure 19d shows two of these row-lines with the second occuring at a spacing of 1.15 nm. When the sample is cooled to room temperature and annealed the pattern in Figure 19d indicates the row-line at 2.3 nm has disappeared while the one at 1.15 nm has nicely developed. The layer reflections which first disappeared at 65°C reappear with much lower intensity (Fig. 19e). This change must be the result of a dramatic symmetry change upon crystallization which confounds the common picture of crystallization from a LC to a solid phase. The conventional

view of the direct build-up of a third dimension of order is not supported by these results. Without synchrotron access, only patterns 19a and 19d were obtainable. These patterns suggest a simple phase change, whereas the intermediate images obtained using the synchrotron indicate this is not the case. Crystallization of the backbone could be a possible explanation but more detailed experiments with labeled compounds have to be carried out to clarify this. If this process is fast the side-groups in a smectic arrangement cannot follow the rearrangement and locking in of the poly(malonate) backbone occurs. The symmetry is disrupted, as a first consequence, leading to the disappearance of the sharp Bragg spots. Upon subsequent annealing the interaction between side-groups dominates and the symmetry is rebuilt. A calculation of the correlation length using the Scherrer equation leads to a 3 to 4 times lower value for the crystalline phase (50.0 nm for the S_A phase and 15.0 nm for the crystalline phase). This is due to a breakdown of the smectic domains into smaller crystallites.

Although the crystallization is a fast process for this polymer, the orientation is retained in the crystalline phase. With *d*-spacing and intensity data from more than 30 reflections it was possible to calculate a unit cell and the positions of side-groups within the packing. Single crystal data from low molecular weight malonates with the same side-groups were used as model compounds to develop the packing of the polymer [108].

X-ray patterns of a poly(malonate) with a shorter spacer $n = 7$, compound VIII are shown in Figure 20(a–c). At 125°C upon cooling, the nematic phase is reached as shown in Figure 20a. Further cooling into the smectic A phase leads to Figure 20b with a strong third order reflection from the smectic layers with a spacing of 3.0 nm. Upon crystallization, a split of the first and second order occurs. The third order reflection is not affected by this split. The first order of the original S_A-phase is still present along with the split reflections. The sharp well-defined reflections are accompanied by diffuse scattering maxima at higher scattering angles near the wide angle crescents. It can be concluded that an additional sub-structure is present which is due to weaker correlated undulations of the layers as also seen for other side-group polymers [89]. A three-fold symmetry is manifested in the strong third order reflection while the first two orders are split in the final semi-crystalline phase. A calculation of the unit cell from 12

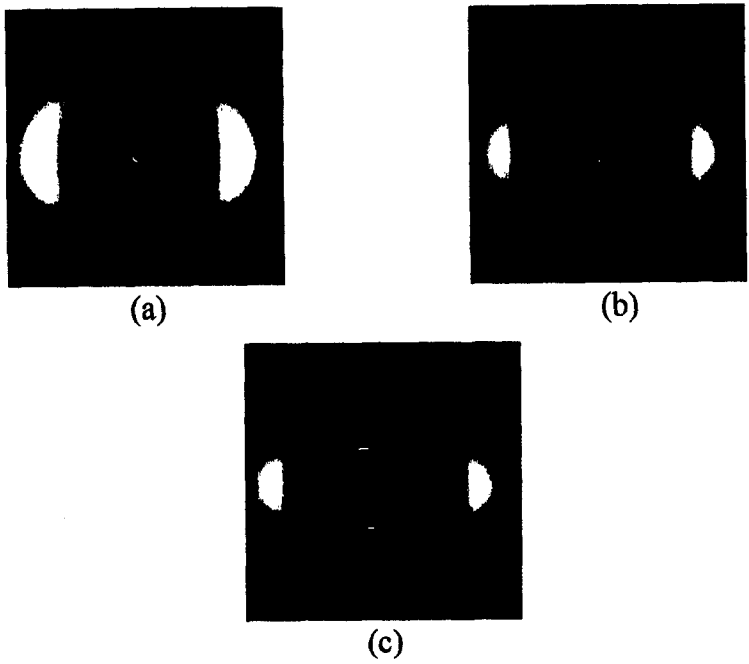

FIGURE 20 X-ray patterns of aligned compound VIII (a) in the nematic phase at 125°C, (b) in the smectic phase at 105°C, and (c) in the crystalline phase at 50°C.

reflections leads to $a = 3.621$, $b = 0.427$, $c = 3.055$ nm and $\beta = 95.6°$. A three-fold symmetry can be constructed by a translation of mesogens of a third of 3.0 nm along c. With a repeating unit for the backbone of 1.2 nm, three of these steps build a package and define the a-dimension of 3.6 nm. The third dimension is not well defined and only local order is present as established in the diffuse wide angle crescent. A schematic of this packing is shown in Figure 21.

The third poly(malonate), compound IX, has a biphenyl group as a mesogenic core and an 8 carbon spacer. A nematic phase with two weak scattering maxima along the electric field as shown in Figure 22 (a–d) is observed initially at 90°C. Cooling into the smectic phase at 68°C leads to an increase of the intensity of these maxima as shown in Figure 22b. Very strong narrow Bragg spots are present with very strong first and weak second order reflections with a smectic layer

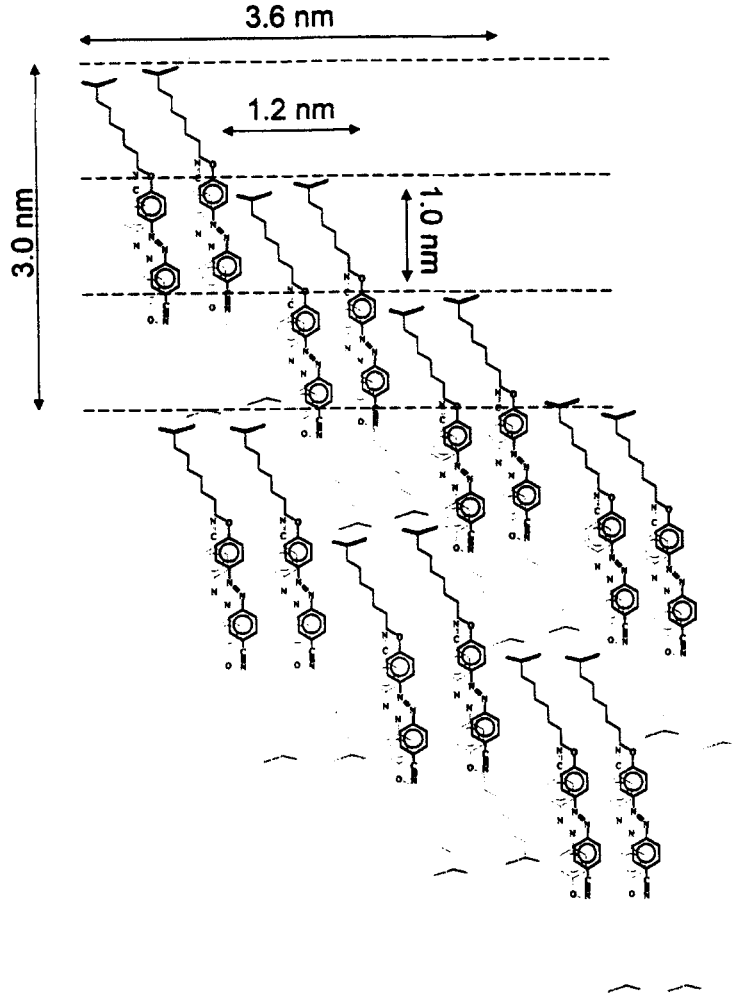

FIGURE 21 Schematic of packing for compound VIII in the semi-crystalline phase.

dimension of 4.2 nm which corresponds to 1.5 times the value of the side-group length (2.7 nm including backbone). When cooling to 50°C, a diffuse third order grows in. Further cooling to 35°C leads to the image shown in Figure 22d. Up to 10 orders to layer reflections can be seen. A split of about 15° indicates a tilt of the mesogens within the layers. The diffuse scattering maxima are still present and also exhibit

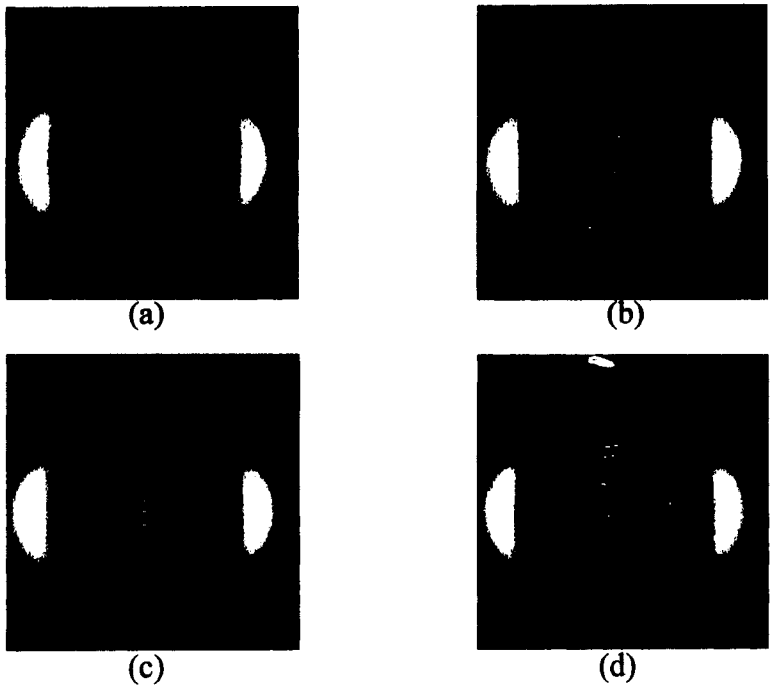

FIGURE 22 X-ray patterns of aligned compound IX (a) in the nematic phase at 90°C, (b) in the smectic phase at 68°C, (c) in the smectic phase at 50°C, (d) in the crystalline phase at 35°C.

a split off the meridian. The splitting angle is larger than 15° and implies two different structures exist at this temperature. A drawn fiber or a powder sample cooled down from the LC phase to room temperature immediately leads to a split of the wide angle reflections after short annealing times. Under the applied electric field, crystallization is hindered and no split into several reflections can be seen even after annealing at 45°C.

For all three compounds, quantitative information regarding the microstructural packing can be obtained. A plot of the orientation parameter *versus* temperature for compound VIII is shown in Figure 23. Similar trends were observed for the other compounds. The orientation parameter increases up to a value of about $S_d = 0.8$ which is common for smectic polymers. The *d*-spacing of the wide angle reflection

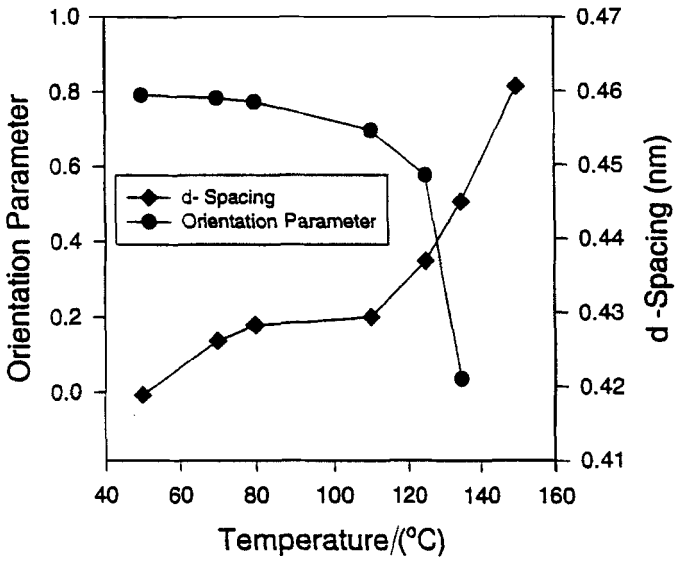

FIGURE 23 Changes of orientation parameter and *d*-spacing upon cooling for compound VIII.

decreases as expected. The correlation length of smectic domains for the polymers is about 50.0 – 60.0 nm.

The results of electric field aligned comb PLCs studied with the high flux synchrotron X-ray radiation demonstrate that this technique serves as an excellent method to get better insight into the kinetics and dynamics of crystallization processes and short-lived transient states. Not only can one dimensional data be followed as a function of time and temperature, but two dimensional fiber patterns of highly oriented polymers necessary for unit cell calculations can be obtained in time- and temperature resolved form.

5.4. Network PLCs

Recently there has been significant interest in polymer networks and thermosets for several applications. Network PLCs combine high dimensional stability and mechanical orientability typical of polymer networks with the unique anisotropic behavior of liquid crystals [109]. With this respect, great attention is presently being addressed to the

synthesis of highly crosslinked networks as both materials for nonlinear optics and electronic packaging and as structural matrix materials for advanced composites [110–115]. For these highly demanding applications, it is essential to develop polymeric materials with optimized structures and precisely controlled architectures. Our research on network PLCs has recently focused on mesophase-forming dicyanate and epoxy esters which can be cured into LC triazine or epoxy networks [111, 116, 117]. The ability of liquid crystals to self order into supramolecular structures capable of being macroscopically oriented by external electric and magnetic fields is transferred to these thermoset systems.

Our goal in this study was to create a molecular system where one could not only align the components in external fields but also selectively control and lock-in the direction of alignment by network formation. Materials treated in this way would possess physical and chemical properties that are very different along each orientation and one could conceive of using photochemistry to form films with order and orientation set in specified regions. By establishing orientation for the dicyanates in a controlled fashion, the properties of such a film can be varied *on demand* prior to crosslinking using only one chemical precursor to form new materials with tunable transport, optical and mechanical properties. These properties are retained even at high temperatures due to the nature of the network [118].

The chemical structure and thermal transitions of the compounds discussed in this section are shown in Figure 24. Dicyanate compounds X and XI cure to a network after melting into the isotropic or liquid crystalline phase. As shown, crosslinking XIa yields network XIb. Diamines are used for crosslinking the epoxy compounds XII and XIII.

The stepwise curing of dicyanate oligomers into high molar mass polymers has been carefully monitored by time-resolved FTIR measurements to get details of the temperature/time dependence and kinetics of the crosslinking reaction. With additional DSC experiments an optimal curing temperature of 190°C was obtained for time-resolved X-ray investigations. These systems were designed to possess a low crossover frequency as discussed earlier. Fields of 1–2 V/μm were applied and the frequency again varied from 1 Hz to 10,000 Hz.

The curing reaction reaches a gelation point in about one hour for compound X and within this time range it is possible to switch the

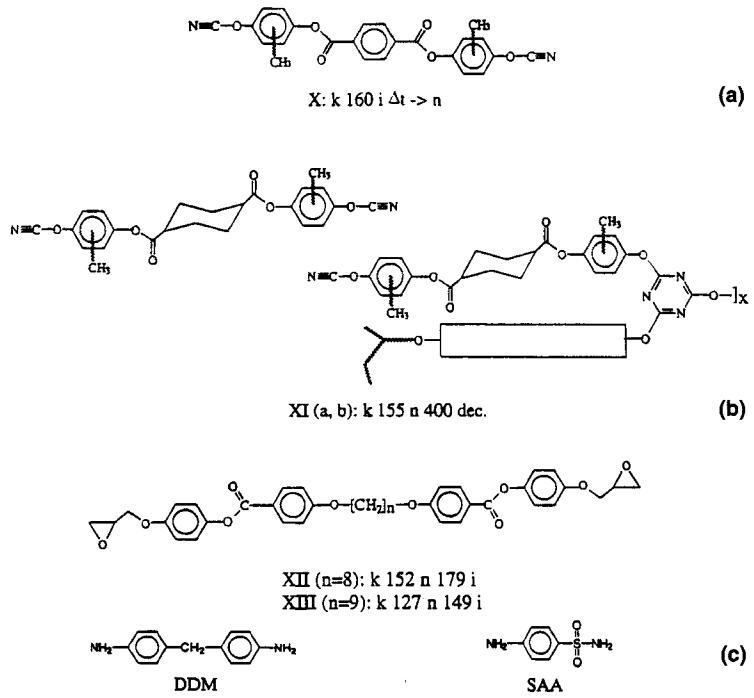

FIGURE 24 Dicyanate with terephthalic acid ester unit-compound X; dicyanate with cyclohexyl unit-compound XIa; triazine network formed by heat treatment of XIa-compound XIb; and epoxy ester with twin structures (compounds XII and XIII) and diamines used for crosslinking.

orientation back and forth by changing the frequency. The prerequisite for such behavior is the ester group present in the molecules similar to compounds IV – VI discussed earlier. Thus, it is possible to selectively control the ending orientation frozen into the completely cured system. Since the curing reaction for compound XIa with the flexible cyclohexyl-group in the mesogenic core is much faster than compound X, the resulting alignment is poor and the orientation is locked in within 2 min. It is also possible to change the final orientation by starting the reaction with either a high or low frequency. A switching of the nematic director cannot be induced during the curing reaction. A preset frequency has to be chosen to set either a parallel or perpendicular orientation of molecules to the electric field. Analysis of the time dependent images leads to the results shown in Figure 25 for compound X. The dual

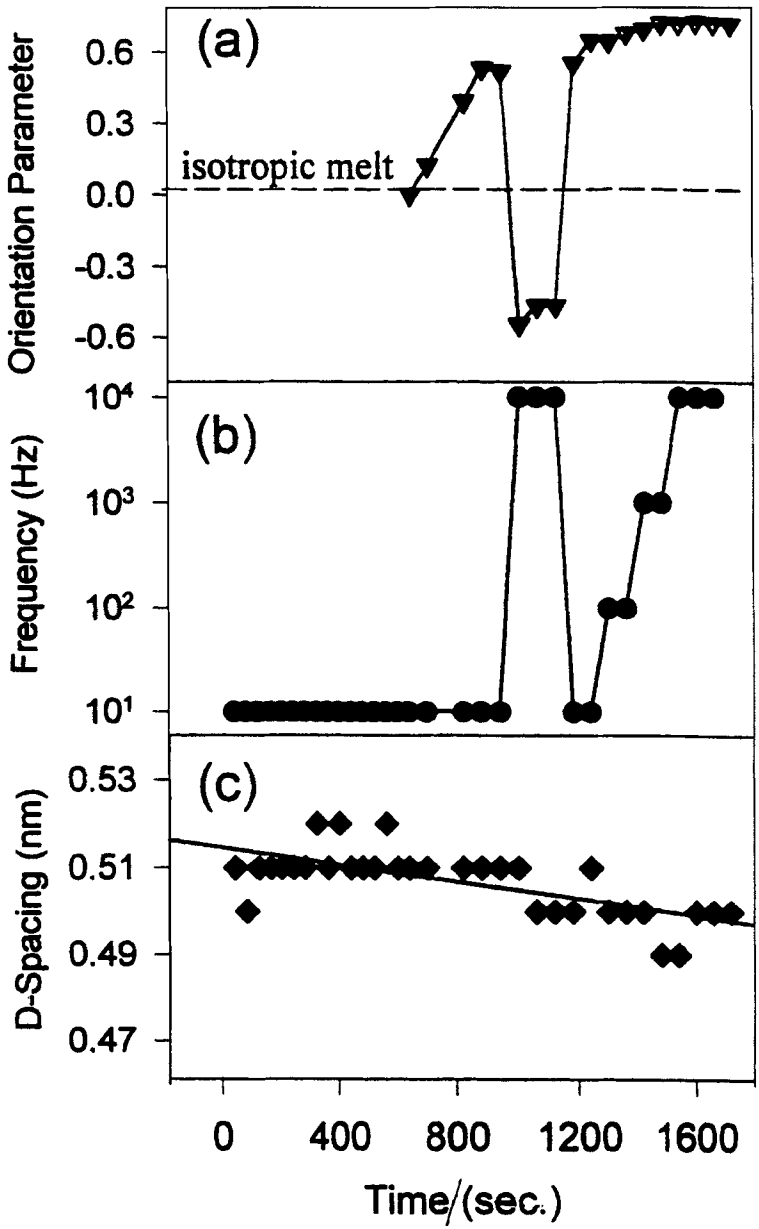

FIGURE 25 The results of a time-resolved experiment for compound X held isothermally at 190°C. The orientation parameter (a) frequency, (b) and wide angle *d*-spacing (c) as a function of time.

frequency addressing property is shown by the change in the sign of the orientation parameter when frequency is changed for 10 Hz to 10,000 Hz. Figure 25a shows the orientation parameter calculated from azimuthal scans through the wide angle reflection. For better comparison, perpendicular alignment has been calculated with a new reference direction 90° to the applied field and the value obtained has been given a negative sign. Figures 25 b, c show applied frequency and changing *d*-spacing respectively for the curing thermoset. After an induction period of about 500 sec, the curing material orients in the applied electric field and the orientation parameter increases gradually with time (Fig. 25a). A change in frequency to 10,000 Hz at about 1000 sec induces a flip in orientation evident in the negative value for the orientation parameter. A switch back to 10 Hz leads to reorientation to a positive value. After this time an increase of the applied frequency to higher values (25b) starting at 1200 s does not change the nematic director and the orientation of the sample is finally locked in. A stepwise change in frequency to 10,000 Hz does not change the orientation. The *d*-spacing of the wide-angle reflection decreases as the curing reaction proceeds from a value of 0.53 to 0.50 nm indicating densification of the network during crosslinking which is independent of orientation. Longer curing times lead to an increase in density of crosslink sites and above the gelation point a reorientation is not possible anymore.

The schematic drawing of Figure 26a summarizes these results and also shows the X-ray patterns of networks for the compounds shown in Figure 24a, b after curing at 10 Hz (Fig. 26b) and 10 kHz (Fig. 24) and 10 kHz (Fig. 26c) electric fields. From these observations, orientation parameters were calculated. The calculations were carried out with the appropriate corrections for uniaxial oriented fibers after background correction. The *d*-spacings calculated from the wide angle reflections for compound X was 0.52 nm and 0.48 nm for compound XI. It can be concluded that the orientation of compound X is superior to that of the more flexible and faster curing cyanate, compound XI. The calculated orientation parameter of 0.6 for cured compound X is comparable to that typically obtained for oriented nematic phases while compound XI exhibits a relatively low value of 0.35. However, the radial width of the WAXD reflection is narrower for compound XI. This information is important as the radial width of a reflection offers information about the domain size of the nematic

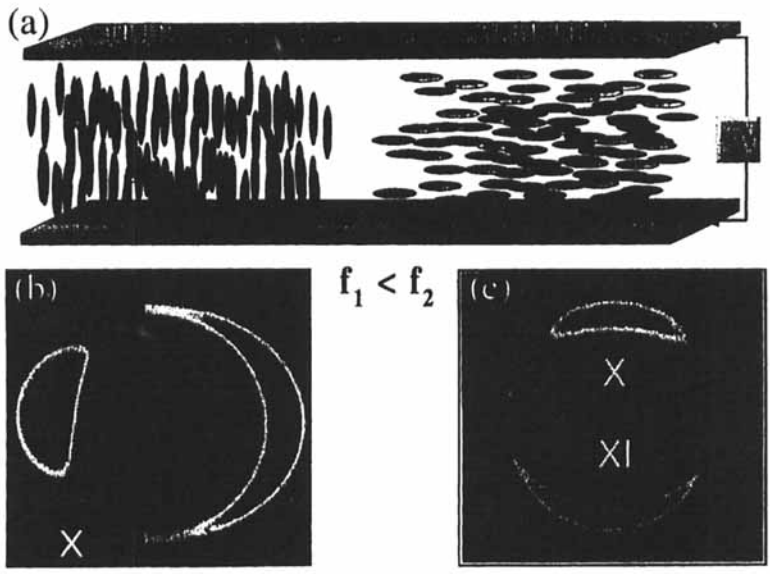

FIGURE 26 Schematic of orientation (a) of the molecules for both dicyanate compounds (X and XI) aligned at 10 Hz (b) and 10,000 Hz (c).

phase of a polymer. Although the orientation for compound XI is weaker, its resulting domain size is larger. Once orientation is achieved, network formation locks in this arrangement and holds it well above the glass transition temperature of the networks.

A different behavior is observed from the E-field alignment of the twin epoxy thermosets, compounds XII and XIII. No dual frequency behavior in the frequency window studied was detected for either the monomers or the networks. The epoxy monomers were easily oriented by the electric field at both 10 Hz and 10 kHz. Both monomers exhibit only a nematic phase with the nematic director along the applied field direction. Curing with diamines SAA and DDM shown in Figure 22 leads to the formation of smectic phases [116]. These cured thermosets show orientation of the mesogens perpendicular to the applied field direction, which is the opposite behavior as observed for the monomers. Figure 27 shows the curing of compound XII with diamine SAA aligned at 10,000 Hz. The strong tendency of this system to form smectic phases can be seen from the rapid growth of the small angle reflection. The

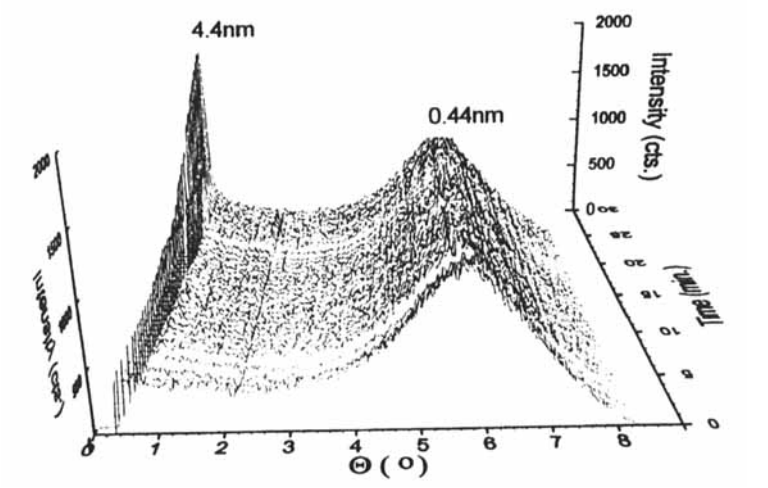

FIGURE 27 Time-resolved increase of smectic domains for compound XII cured with SAA at 175°C.

epoxy monomer XIII cured with diamine DMM exhibits similar behavior. Although the director of the LC phase of this thermosetting system cannot be changed by frequency, the addition of diamines as curing agents leads to a perpendicular alignment of the final networks suggesting a considerable difference in the curing of twin LC network compounds in an electric field.

In summary, two systems of thermosets have been successfully investigated at the synchrotron. A dicyanate system is able to crosslink without additional agents, just by heating into the isotropic or liquid crystalline melt. Due to the presence of the proper ester group and an isomeric mixture a dual frequency behavior was observed in the experimental limit of our setup. The curing reaction enabled us to "lock" in the desired orientation by aligning with the proper frequency. This orientation is stable indefinetely at temperatures below the onset of decomposition. A different thermoset system based on epoxy monomers cured with aromatic diamines with a twin-mesogenic structure showed a strong tendency to form smectic ordering. Although ester groups are present in this case, no switch in orientation was observed, although an important effect of the electric field was demonstrated. Whereas epoxy monomers show a homeotropic alignment, networks formed from these compounds show planar orientation. The complex curing chemistry of

this system leads to a very different behavior compared to the dicyanates. Thus, the synchrotron serves as a valuable tool to monitor structural changes induced by changes in molecular structure. The ability to monitor in real-time the dynamics of the curing and alignment simultaneously allows for a much better understanding of changes taking place.

6. FUTURE PERSPECTIVES

This article has sought to demonstrate the methodology this technique promises for the fundamental investigation of the static and dynamic orientation and alignment behavior of MLCs and PLCs under applied fields. The effects of electric fields on LC organization and the switching behavior of these materials are not fully clear from the molecular organizational perspective. The effects of ion flow as well as subtleties in dielectric properties have yet to be explored. The prospects are good for additional fundamental information about liquid crystals to be obtained from such studies.

An area for productive exploration is the use of X-ray surface techniques to probe the organization of the surface region of LC materials under an applied electric field. It has already been established that the effect of surfaces on LC self-assembly is quite pronounced. Studies have in fact shown that low order LC materials exhibit induced smectic-like order at the air-LC surface. X-ray surface techniques using a high flux source can readily examine such behavior and indicate the extent of organization as well as orientation at the surface in real-time. Labelling of terminal chemical moities will provide insight into dynamics. Another area which has been briefly reviewed in this review is the real-time monitoring of chemical reactions within LC architectures. It should be appreciated that we are in fact following molecular level changes caused by polymerization and the induction of liquid crystallinity. Real-time X-ray diffraction provides a unique opportunity to examine these chemical changes and may in fact offer a means of probing aspects of chemistry not readily studied by other techniques.

Perhaps the most exciting prospect for time resolved X-ray diffraction will be its combination with other *in-situ* techniques.

Already both DSC and FTIR have been paired with synchrotron diffraction in non-liquid crystalline systems. These techniques have enabled the crystallization processes to be studied in great detail. By coupling these techniques to X-ray diffraction it is possible to obtain detailed molecular level information while at the same time examining a more macroscopic response. In the case of liquid crystals, techniques for probing alignment and LC order are of interest. In addition, the study of photochemical reactions and optical response are also of potential use. Since light can induce chemical reactions, the study of photocuring and network formation is an area of potential investigation. Already we have seen that changes in molecular organization can be monitored during the curing of LC thermosets. Coupled with photochemistry, we can examine the effect these changes have on structure. In the area of polymer dispersed LC displays both changes to molecular organization during formation of the dispersed phase can be monitored and at the same time *via* SAXS we can observe the phase separation process. As a final example, simultaneous corona poling and subsequent optical measurements and time-resolved diffraction should faciliate the coupling of molecular level changes to macroscopic optical properties.

From the experimental viewpoint, the fields of real time and *in situ* synchrotron studies are in a revolution. The old detectors (film, video cameras, proportional counters) are still widely used, but are rapidly being displaced by image plates [119] and CCD detectors, which offer tremendous advantages in rapid acquisition of digital 2-D data and of dynamic range. But even these detectors are likely to be soon replaced by direct signal, rapid readout CCD's and the avalanch photo diode detectors [120]. The construction of third generation synchrotron sources, such as the Advanced Photon Source at Argonne National Lab and the European Synchrotron Radiation Facility at Grenoble has driven a new generation of detector development, and commercial implementation of these systems cannot be far behind.

As the detector speed and dynamic range have increased, so has the brightness of the synchrotron sources, and the APS will soon be the brightest in the world [121]. With increased flux available at useful diffraction wavelengths ($0.5 < 1 < 2.0$ Å), the size of the sample irradiated can be considerably reduced. With techniques such as tapered lead glass capillaries, a volume of diffracting material as small

as $5 \times 10^{-3}\,\mu m^3$ can be targeted, as was demonstrated for diffraction from a thin single crystal of gold [122] or from a single synthetic or natural fiber [123, 124]. Diffraction from a small region of a single polymer crystal is certainly feasible, and one can predict an experiment seeking to obtain a diffraction pattern from a single domain or even a single defect in a self-supported LC film (*e.g.*, thickness 1 mm, area $(5\,\mu m)^2$, or from a total volume of $25\,\mu m^2$).

Time resolution is certainly possible to the nanosecond regime by timing the exposure to coincide with the arrival of X-rays from a single bunch of electrons (or positrons) traveling around the ring, *e.g.*, at CHESS, there are seven bunches per fill, traveling around the ring with a cycle time of 2.5 ms, with a bunch length of 160 ps. Some synchrotrons can be operated in single bunch mode with high purity, making possible experiments in stroboscopic topology and nuclear diffraction. Feasibility has been demonstrated for "single shot" protein Laue patterns [125]. Other techniques are available for even faster time resolution, including pulsed X-ray systems with picosecond resolution [126]. New methods continue to be developed, including a recent prediction of the ability to modulate a beam with a crystal modulated by a standing acoustic wave, where the frequency of the modulated intensity of the diffracted beam from the crystal is many times faster than the acoustic frequency, *i.e.*, for 100 MHz acoustic freq, a 100-fold modulated intensity will occur at 50–100 ps! [127]. This type of high speed X-ray modulation will allow, in principle, the measurement of changes in structure in excited states, as was demonstrated in a static experiment only with great difficulty [128]. The coupling of additional applied fields to a system under study opens us considerably new territory for exploration, since one can now feasibly combine X-rays, light (including pulsed laser beams), chemical reactions, optical spectroscopy, calorimetry, mechanical deformation, rheology, and electric and magnetic fields in the same experiment.

The final requirement is the precise control of the sample illumination location. Recently, controlled micromanipulation of samples has been elegantly demonstrated for the case of thin spherulitic polymer films, where a 15 by 15 array of WAXS images was taken from an area of the center of a spherulite approximately 150 μm by 150 μm using a beam diameter of about 10 μm. The experiment generated 225 patterns recorded in about 1s each, resulting in a graphic

display of the center of a spherulite's orientation distribution, which graced the cover of the Journal of Synchrotron Radiation, 1 November 1995 [129]. Also demonstrated was software capable of analyzing orientation functions and degree of crystallinity from sequential patterns, a capability absolutely essential to further (nonmanual) analysis of *e.g.*, 10,000 patterns from a 1×1 mm sized specimen.

The infrastructure is now available to exploit these burgeoning technologies, and the problems in liquid crystal physics and chemistry are certainly worthy of the effort. All that remains is to formulate experiments commensurate with these advances, and to expend the time and money to do it.

Author's Note

This article was written as a book chapter and submitted to the respective editors in the middle of 1996. Due to conditions out of the editors and authors control, the article published here is the same as was submitted previously. No opportunity to make references or experiments current was offered or subsequently attempted. The world of synchrotron radiation and its use to monitor dynamic behavior has continued to evolve and advance at a rising pace over the last 3+ years. Elegant real-time experiments in the field of polymers and liquid crystals have been reported in the literature and we apologize to all whose work has not been referenced in this work. At the original time of submission, the contents of this article, both the experimental results and references, were both current and state-of-the-art.

Acknowledgements

The authors thank all colleagues who have spent many a sleepless night collecting data. Particular thanks to Dr. S. G. McNamee, Dr. D. T. Grubb, Mr. C. M. McHugh and Mr. Atsushi Shiota. Many thanks to the CHESS staff past and present who have helped solve innumerable problems.

References

[1] Bark, M., Schulze, C. and Zachmann, H. G. (1985). *Am. Chem. Soc. Polymer Prep.*, **23**, 1109.

[2] Galambos, A. F. (1989). *Ph. D. Dissertation*, Princeton University.
[3] Russell, T. P. and Koberstein, J. T. (1986). *J. Polymer Sci. Phys.*, **19**, 714.
[4] Ungar, G. and Feijoo, J. L. (1990). *Mol. Cryst. Liq. Cryst.*, **180B**, 281.
[5] Bras, W., Derbyshire, G. E., Bogg, D., Cooke, J., Elwell, M. J., Komanschek, B. U., Naylor, S. and Ryan, A. J. (1995). *Science*, **267**, 996.
[6] Clements, J., Zachmann, H. G. and Ward, I. M. (1988). *Polymer*, **29**, 1929.
[7] Zachmann, H. G. (1995). *Nucl. Instr. Methods*, **97**, 209.
[8] Haswell, R., van Mechelen, J. B., Mensch, C. T. J. and de Grot, H. (1995). *Nucl. Instr. Meth.*, **97**, 242.
[9] Hsiao, B. S., Gardner, B. H., Wu, D. Q. and Chu, B. (1993). *Polymer*, **34**, 3986.
[10] Cooke, J., Ryan, A. J. and Bras, W. (1995). *Nucl. Instr. Meth.*, **97**, 269.
[11] Rastogi, S. and Ungar, G. (1992). *Macromolecules*, **25**, 1445.
[12] Bras, W., Derbyshire, G. E., Ryan, A. J., Mant, G. R., Manning, P., Cameron, R. E. and Mormann, W. (1993). *J. Phys. IV*, **3**, 447.
[13] Li, Y., Gao, T. and Chu, B. (1992). *Macromolecules*, **25**, 1737.
[14] Nojima, S., Kato, K., Ono, M. and Ashida, T. (1992). *Macromolecules*, **25**, 1922.
[15] Zachmann, H. G. and Wutz, C. (1993). *NATO ASI Ser., Ser. C*, **405**, 403.
[16] Tashiro, K. (1995). *Acta Polym.*, **46**, 100.
[17] Jonas, A. M., Russell, T. P. and Yoon, D. Y. (1994). *Coll. Polymer Sci.*, **272**, 1344.
[18] Cakmak, M., Teitge, A., Zachmann, H. G. and White, J. L. (1993). *J. Polymer Sci. Phys.*, **31**, 371.
[19] Blundell, D. J., Mahendrasingam, A., McKerron, D., Turner, A., Rule, R., Oldman, R. J. and Fuller, W. (1994). *Polymer*, **35**, 3875.
[20] Mahendrasingam, A., Martin, C., Jaber, A., Hughes, D., Fuller, W., Rule, R., Oldman, R. J., MacKerron, D. and Blundell, D. J. (1995). *Nucl. Instr. Meth.*, **97**, 238.
[21] Rule, R. J. and Nye, T. M. W. (1995). *Nucl. Instr. Methods*, **97**, 248.
[22] Schmack, G., Beyreuther, R., Haubler, L., Tidick, P. J., Zachmann, H. G. and Koch, M. H. J. (1994). *Macro. Chem. Phys.*, **195**, 3523.
[23] Dreher, S., Zachmann, H. G., Riekel, C. and Engstrom, P. (1995). *Macromolecules*, **28**, 7071.
[24] Ryan, A. J., Hamley, I. W., Bras, W. and Bates, F. S. (1995). *Macromolecules*, **28**, 3860.
[25] Ying, Q., Chu, B., Wu, G., Linliu, K., Gao, T., Nose, T. and Okada, M. (1993). *Macromolecules*, **26**, 5890.
[26] Wang, J., Alvarez, M., Zhang, W., Wu, Z., Li, Y. and Chu, B. (1992). *Macromolecules*, **25**, 6943.
[27] Wolff, T., Burger, C. and Ruland, W. (1994). *Macromolecules*, **27**, 3301.
[28] Wolff, T., Burger, C. and Ruland, W. (1993). *Macromolecules*, **26**, 1707.
[29] Nojima, S., Nakano, H., Takahashi, Y. and Ashida, T. (1994). *Polymer*, **35**, 3479.
[30] Wu, G., Ying, Q. and Chu, B. (1994). *Macromolecules*, **27**, 5758.
[31] Naylor, S., Bras, W., Derbyshire, G., Mant, G. R., Bogg, D. and Ryan, A. J. (1995). *Nucl. Instr. Meth.*, p. 253.
[32] Ryan, A. J., Willkomm, W. R., Bergstrom, T. B., Macosko, C. W., Koberstein, J. T., Yu, C. C. and Russell, T. P. (1991). *Macromolecules*, **24**, 2883.
[33] Caffrey, M. (1991). *Trends Anal. Chem.*, **10**, 156.
[34] Caffrey, M. (1989). *Topics in Current Chemistry*, **151**, 75.
[35] Kriechbaum, M., Rapp, G., Hendrix, J. and Laggner, P. (1989). *Rev. Sci. Instrum.*, **60**, 2541.
[36] Chung, H. and Caffrey, M. (1992). *Biophys. J.*, **63**, 438.
[37] Quinn, P. J. (1992). *Maku*, **17**, 379.
[38] Hirai, M., Takizawa, T., Yanuki, S., Hirai, T. and Ueki, T. (1995). *Phys. Rev. E*, **51**, 1263.

[39] Clerc, M., Laggner, P., Levelut, A.-M. and Rapp, G. (1995). *J. Phys. II France*, **5**, 901.
[40] Cunningham, B. A., Bras, W., Lis, L. J. and Quinn, P. J. (1994). *J. Biochem. Biophys. Meth.*, **29**, 87.
[41] Warriner, H. E., Idziak, S. H. J., Kraiser, K. E. and Safinya, C. R. (1994). *Am. Chem. Soc. Polymer Prep.*, **35**, 641.
[42] Michalczyk, M. J., Farneth, W. E. and Vega, A. J. (1993). *Chem. Mat.*, **5**, 1687.
[43] Bruinsma, R. F. and Safinya, C. R. (1993). *MRS Symp. Proc.*, **290**, 3.
[44] Safinya, C. R., Sirota, E. B. and Plano, R. J. (1991). *Phys. Rev. Lett.*, **66**, 1986.
[45] Plano, R. J., Safinya, C. R., Sirota, E. B. and Wenzel, L. J. (1993). *Rev. Sci. Instrum.*, **64**, 1309.
[46] Pople, J. A., Mitchell, G. R. and Chai, C. K. (1994). In: *Advances in X-ray Analysis* (Ed. Predecki, P. K.), Plenum, New York, p. 531.
[47] Idziak, S. H. J., Safinya, C. R., Sirota, E. B., Bruinsma, R. F., Liang, K. S. and Israelachvili, J. N. (1994). *ACS Symp. Ser.*, **578**, 288.
[48] Zachmann, H. G. and Thiel, S. (1992). *Trends Non-Cryst. Solids*, p. 245.
[49] Delvin, A., Ober, C. K. and Bluhm, T. L. (1989). *Macromolecules*, **22**, 498.
[50] Ober, C. K. and Bluhm, T. L. (1986). *Polymer Bull.*, **15**, 233.
[51] Ober, C. K., Delvin, A. and Bluhm, T. L. (1990). *J. Polymer Sci.*, **28**, 1047.
[52] Delvin, A., Ober, C. K. and Bluhm, T. L. (1988). *PMSE*, **58**, 1029.
[53] Cohen, Y., Buchner, S., Zachmann, H. G. and Davidov, D. (1992). *Polymer*, **33**, 3811.
[54] Flores, A., Ania, F., Calleja, F. J. B. and Ward, I. M. (1993). *Polymer*, **34**, 2915.
[55] Nolan, S. J., Broomall, C. F., Bubeck, R. A., Radler, M. J. and Landes, B. G. (1995). *Rev. Sci. Instrum.*, **66**, 2652.
[56] Radler, M. J., Landes, B. G., Nolan, S. J., Broomall, C. F., Chritz, T. C., Rudolf, P. R., Mills, M. E. and Bubeck, R. A. (1994). *J. Polymer Sci. Phys.*, **32**, 2567.
[57] Noh, D. Y., Brock, J. D., Fossum, J. O., Hill, J. P., Nuttall, W. J., Litster, J. D. and Birgeneau, R. J. (1991). *Phys. Rev. B*, **43**, 842.
[58] Harris, Q. J., Noh, D. Y., Turnbull, D. A. and Birgeneau, R. J. (1995). *Phys. Rev. E: Stat. Phys.*, **51**, 5797.
[59] Sirota, E. B., Pershan, P. S., Amador, S. and Sorensen, L. B. (1987). *Phys. Rev. A: Gen. Phys.*, **35**, 2283.
[60] Brock, J. D., Aharony, A., Birgeneau, R. J., Evans-Lutterodt, K. W., Litster, J. D., Horn, P. M., Stephenson, G. B. and Tajbakhsh, A. R. (1986). *Phys. Rev. Lett.*, **57**, 98.
[61] Safinya, C. R., Clark, N. A., Liang, K. S., Varady, W. A. and Chiang, L. Y. (1985). *Mol. Cryst. Liq. Cryst.*, **123**, 205.
[62] Safinya, C. R., Sirota, E. B., Bruinsma, R. F., Jeppesen, C., Plano, R. J. and Wenzel, L. J. (1993). *Science*, **261**, 588.
[63] Moncton, D. E., Pindak, R., Davey, S. C. and Brown, G. S. (1982). *Phys. Rev. Lett.*, **49**, 1865.
[64] Pershan, P. S. (1990). *Faraday Discuss.*, **89**, 231.
[65] Haase, W. (1989). In: *Side Chain Liquid Crystal Polymers* (Ed. McArdle, C. B.), Blackie, Glasgow, p. 309.
[66] Blinov, L. M. (1983). *Electro-Optical and Magneto-Optical Properties of Liquid Crystals*, John Wiley and Sons, NY.
[67] Donald, A. M. and Windle, A. H. (1992). *Liquid Crystalline Polymers*, University Press, Cambridge.
[68] McArdle, C. B. (1989). In: *Side Chain Liquid Crystal Polymers*, Blackie, Glasgow, p. 448.
[69] Ortler, R., Brauchle, C., Miller, A. and Riepl, G. (1989). *Makromolecular Chemie, Rapid Communications*, **10**, 5.
[70] Prasad, P. N. and Williams, D. J. (1991). In: *Introduction to Nonlinear Optical Effects in Molecules and Polymers*, Wiley-Interscience, NY, p. 320.

[71] Anderle, K., Birenheide, R., Eich, M. and Wendorff, J. H. (1989). *Makromol. Chem. Rapid Commun.*, **10**, 477.
[72] Eichler, H. J., Heppke, G., MacDonald, R. and Schmid, H. (1992). *Mol. Cryst. Liq. Cryst.*, **223**, 159.
[73] Eich, M., Wendorff, J. H., Reck, B. and Rinsdorf, H. (1987). *Makromol. Chem. Rapid Commun.*, **8**, 59.
[74] Meredith, G. R., VanDusen, J. G. and Williams, D. J. (1982). *Macromolecules*, **15**, 1385.
[75] Kaneko, E. (1987). *Liquid Crystal TV Displays*, KTK Scientific Publishers, Tokyo.
[76] Nazemi, A., Williams, G., Attard, G. S. and Karasz, F. E. (1992). *Polymers Adv. Tech.*, **3**, 157.
[77] Haase, W. and Pranato, H. (1984). *Progr. Colloid and Polym. Sci.*, **69**, 139.
[78] Haase, W., Pranato, H. and Brmuth, F. J. (1985). *Ber. Bunsenges. Phys. Chem.*, **89**, 1229.
[79] Plate, N. A., Talroze, R. V. and Shibaev, V. P. (1984). *Pure & Appl. Chem.*, **56**, 403.
[80] Esnault, P., Casquilho, J. P., Volino, F., Martins, A. F. and Blumstein, A. (1990). *Liq. Cryst.*, **7**, 607.
[81] Martins, A. F., Esnault, P. and Volino, F. (1986). *Phys. Rev. Lett.*, **57**, 1745.
[82] Kozak, A., Simon, G. P., Moscicki, J. K. and Williams, G. (1990). *Mol. Cryst. Liq. Cryst.*, **193**, 155.
[83] Kozak, A., Simon, G. P. and Williams, G. (1989). *Polymer Commun.*, **30**, 102.
[84] Haase, W. and Pranato, H. (1985). In: *Polymeric Liquid Crystals* (Ed. Blumstein, A.), Plenum, New York, p. 313.
[85] Pranato, H. and Haase, W. (1983). *Mol. Cryst. Liq. Cryst.*, **98**, 99.
[86] Attard, G. S., Williams, G., Gray, G. W., Lacey, D. and Gemmel, P. A. (1986). *Polymer*, **27**, 185.
[87] Leadbetter, A. J. (1987). In: *Thermotropic Liquid Crystals* (Ed. Gray, G. W.), John Wiley & Sons, Chichester, p. 1.
[88] Noel, C. (1989). In: *Side Chain Liquid Crystal Polymers* (Ed. McArdle, C. B.), Blackie, Glasgow, p. 159.
[89] Davidson, P. and Levelut, A. M. (1992). *Liq. Cryst.*, **11**, 469.
[90] Azaroff, L. V. (1987). *Mol. Cryst. Liq. Cryst.*, **145**, 31.
[91] Gleeson, H. F., Carboni, C. and Morse, A. S. (1995). *Rev. Sci. Instrum.*, **66**, 3563.
[92] McNamee, S. G., Bunning, T. J., Patnaik, S. S., McHugh, C. M., Ober, C. K. and Adams, W. W. (1995). *Liq. Cryst.*, **18**, 787.
[93] McNamee, S. G., Bunning, T. J., McHugh, C. M., Ober, C. K. and Adams, W. W. (1994). *Liq. Cryst.*, **17**, 179.
[94] McNamee, S. G., Galli, G. and Ober, C. K. (1992). *MRS Conf. Proc.*, **248**, Boston, MA, 101.
[95] Shibaev, V. P. and Freidzon, Y. S. (1989). In: *Side Chain Liquid Crystal Polymers* (Ed. McArdle, C. B.), Blackie, Glasgow, p. 260.
[96] Shibaev, V. P., Talroze, R. V., Korobeinikova, I. A. and Plate, N. A. (1989). *Liq. Cryst.*, **4**, 467.
[97] Wang, H., Jarnagin, R. C., Samulski, E. T., Bunning, T. J. and Adams, W. W. (1994). *Am. Chem. Soc. Polymer Prep.*, **35**, 194.
[98] Wang, H., Jin, M. Y., Jarnagin, R. C., Samulski, E. T., Bunning, T. J., Adams, W. W., Cull, B., Shi, Y. and Kumar, S. (1996). *Nature*, in press.
[99] Shi, H. and Chen, S. H. (1994). *Liq. Cryst.*, **17**, 413.
[100] Shi, H. and Chen, S. H. (1995). *Liq. Cryst.*, **18**, 733.
[101] Kreuzer, F. H., Andrejewski, D., Haas, W., Haberle, N., Riepl, G. and Spes, R. (1991). *Mol. Cryst. Liq. Cryst.*, **199**, 345.
[102] Bunning, T. J. and Kreuzer, F. H. (1995). *Trends Polymer Sci.*, **3**, 318.
[103] Bunning, T. J. (1992). *Ph.D. Dissertation*, University of Connecticut.

[104] Bunning, T. J., McNamee, S. G., McHugh, C. M., Patnaik, S. S., Ober, C. K. and Adams, W. W. (1993). *MRS Proc.*, **307**, 311.
[105] Bunning, T. J., Korner, H., Tsukruk, V. V., McHigh, C. M., Ober, C. K., Adams, W. W. (1996). *Macromolecules*, **29**, 8706.
[106] Vertogen, G. and deJeu, W. H. (1988). *Thermotropic Liquid Crystals, Fundamentals*, Springer-Verlag, Berlin.
[107] Korner, H. (1994). *Ph.D. Dissertation*, Universitat Clausthal, Germany.
[108] Korner, H. and Zugenmaier, P. (1993). *Cryst. Res. Technol.*, **28**, 1181.
[109] Gleim, W. and Finkelmann, H. (1989). In: *Side Chain Liquid Crystal Polymers* (Ed. McArdle, C. B.), Blackie, Glasgow, p. 287.
[110] Ou, J. C., Hong, Y., Yen, F. S. and Hong, J. L. (1995). *J. Polymer Sci. Chem.*, **33**, 313.
[111] Barclay, G. G., Ober, C. K., Papathomas, K. I. and Wang, D. W. (1992). *Macromolecules*, **25**, 2947.
[112] Barclay, G. G., Ober, C. K., Papathomas, K. I. and Wang, D. W. (1992). *J. Polymer Sci. Chem.*, **30**, 1831.
[113] Barclay, G. G. and Ober, C. K. (1993). *Prog. Polymer Sci.*, **18**, 899.
[114] Hoyt, A. E. and Benecewicz, B. C. (1990). *J. Polymer Sci. Chem.*, **28**, 3403.
[115] Carfagna, C., Amendola, E., Giamberini, M. and Flippov, A. G. (1994). *Makromol. Chem. Phys.*, **195**, 279.
[116] Shiota, A. and Ober, C. K. (1996). *J. Polymer Sci. Chem.*, **34**, 1291.
[117] Korner, H. and Ober, C. K. (1995). *PMSE*, **73**, 456.
[118] Korner, H., Shiota, A., Bunning, T. J. and Ober, C. K. (1996). *Science*, **272**, 252.
[119] Amemiya, Y. (1990). *Synchrotron Radiation News*, **3**, 21.
[120] Baron, A. Q. R. and Ruby, S. L. (1994). *Nucl. Instr. Meth.*, **343**, 517.
[121] Hasnain, S. S., Halliwell, J. R. and Kamitsubo, H. (1995). *J. Synchrotron Rad.*, **2**, 275.
[122] Bilderback, D. H., Hoffman, S. A. and Thiel, D. J. (1994). *Science*, **263**, 201.
[123] Prasad, K. and Grubb, D. T. (1989). *J. Polymer Sci. Phys.*, **27**, 381.
[124] McNamee, S. G., Ober, C. K., Jelinski, L. W., Ray, E., Xia, Y. and Grubb, D. (1993). In: *Silk Polymers Materials Science and Biotechnology* (Eds. Kaplan, D., Adams, W., Farmer, B. and Viney, C.), American Chemical Society, p. 176.
[125] Revol, J. L. and Plouviez, E. (1994). *Synch. Rad. News*, **7**, 23.
[126] Tomov, I., Chen, P. and Rentzepis, P. M. (1995). In: *Advances in X*-ray *Analysis*, (Eds. Predecki, P.).
[127] Iolin, E. M. (1995). *Acta Cryst. A*, p. 897.
[128] Pressprich, M. R., White, M. A., Vekhter, Y. and Coppens, P. (1994). *J. Am. Chem. Soc.*, **116**, 5233.
[129] Mahendrasingam, A., Martin, C., Fuller, W., Blundell, D. J., MacKerron, D., Rule, R. J., Oldman, R. J., Liggat, J., Riekel, C. and Engstrom, P. (1995). *J. Synchrotron. Rad.*, **2**, 308.